Hydraulic power connection for Ocean Grazer

Dynamic model and component selection of a section of a high-pressure hydraulic power connection for the Ocean Grazer 3.0 and an exploration of Pump as Turbines and generators suitable for the Ocean Battery.

university of groningen / faculty of science and engineering

OCEAN GRAZER

Author: Tijs Richard Paul Papousek

Student Number: S3208508

First supervisor: Prof. dr. A. I. Vakis

Second supervisor: T. M. Kousemaker

BSc Industrial Engineering & Management, Faculty of Science and Engineering

The University of Groningen, 19th of June 2020

university of groningen / faculty of science and engineering

Abstract

It is an enormous challenge in current society to achieve a stable energy supply from renewables. Ocean Grazer is a company that has developed a concept that could contribute to achieving this challenge. To deliver a competitive product, the concept that harvests and stores wave and wind energy must have optimal efficiency. Therefore, the efficiency of a hydraulic system to transport the harvested energy by the Wave Energy Converter to the Ocean Battery is investigated. In this research, the losses in a hydraulic tube and hydraulic motor to transport the harvested energy to the Ocean Battery were determined for varying power inputs and the efficiency in these components was computed. Furthermore, a survey of applicable generators to connect to the hydraulic motor to generate electricity in the Ocean Battery is presented, as well as the advantages and disadvantages of using Pump as Turbines in the Ocean Battery.

Table of Contents

List of abbreviations

WEC	Wave Energy Converter
PAT	Pump as Turbine
SCIG	Squirrel Cage Induction Generator
WRIG	Wound Rotor Induction Generator
DFIG	Doubly Fed Induction Generator
BDFIG	Brushless Doubly Fed Induction Generator
PMIG	Permanent Magnet Induction Generator
PMSG	Permanent Magnet Synchronous Generator
WRSG	Wound Rotor Synchronous Generator

1. Introduction

Renewable energy is one of the main challenges in modern-day society. Currently, fossil fuels are frequently used as a source of energy. However, as commonly known, when fossil fuels are burnt, they produce large amounts of harmful gases such as carbon dioxide. This gas is the biggest culprit of the current global warming trend. Therefore, a switch to renewable energy is vital for the future of planet earth (Shahzad, 2012). The Danish, German, and Dutch power grid operators have decided to cooperate and agreed to develop a large renewable energy electricity system in the North Sea. This North Sea Wind Power Hub should be able to supply 150 GW of power by 2040 (North Sea Wind Power Hub, 2019). To realise this, one of the challenges is the storage and generation of renewable energy to be able to provide a continuous power supply to consumers. The Ocean Grazer concept is one potential solution to this problem.

Ocean Grazer Holding B.V. is a small high-tech company specialised in capturing and storing offshore renewable energies. The company has created a concept, depicted in Figure 1, that is designed to capture renewable energy from ocean waves and store the energy on-site. This can then be supplied whenever it is demanded. The concept consists of three different main parts: a Wave Energy Converter (WEC), a storage system and a wind turbine. Ocean Grazer has already worked on this concept for several years and has now arrived at the third design, the Ocean Grazer 3.0. The WEC, storage system and the wind turbine together form the Ocean Grazer 3.0, which allows the harvesting and storing of wave and wind energy.

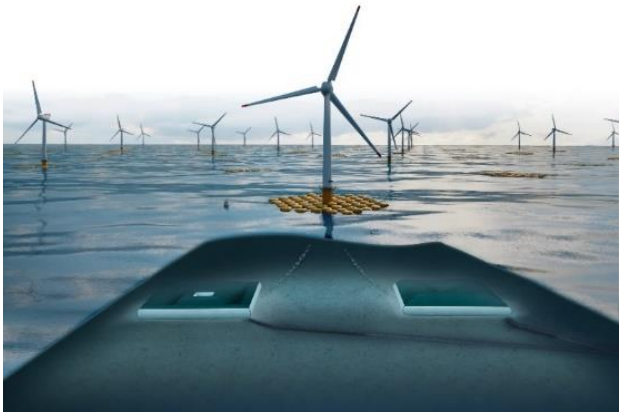

Figure 1: Overview of the OG concept (van Rooij, 2020).

This research will elaborate on a high-pressure hydraulic connection from the WEC to the storage system, called the Ocean Battery. The WEC must supply fluid power and transport this through a hydraulic tube to the Ocean Battery, which is fixed at the sea bottom. In the Ocean Battery, the power must be converted to electrical or potential energy. By investigating a high-pressure hydraulic connection, the efficiency of such a system can be determined for Ocean Grazer. Ocean Grazer could then examine whether this is more efficient than the current electrical system connecting the WEC and the Ocean Battery which they are considering.

The report initiates with an explanation of the problem, its stakeholders, the system and the scope. Thereafter, an objective is expressed, and research questions were phrased, followed by methods and tools. Next, a literature survey is presented about

components relevant in the described system. Consequently, a model that represents the system is added, partially validated, and simulated for the system described. Finally, a discussion and a conclusion are presented.

2. Problem Context

As stated in the introduction, Ocean Grazer makes use of a WEC to harvest energy from waves and this is then to be stored in the Ocean Battery.

The working principle of the current Ocean Battery is as follows and can be seen in Figure 2 and Figure 3 below. From the round rigid reservoirs, water can be pumped into a flexible bladder on top, this will be done either with a separate pump and turbine or with a Pump as Turbine (PAT). The water in the flexible bladder is stored as potential energy due to the hydrostatic overpressure of the sea. If the energy is needed, the water in the flexible bladder can be discharged and flows back to the rigid reservoirs through the turbine or PAT. The turbine or PAT is attached to a generator that can generate electricity. Then, the electricity can be transported to the mainland to be used by consumers.

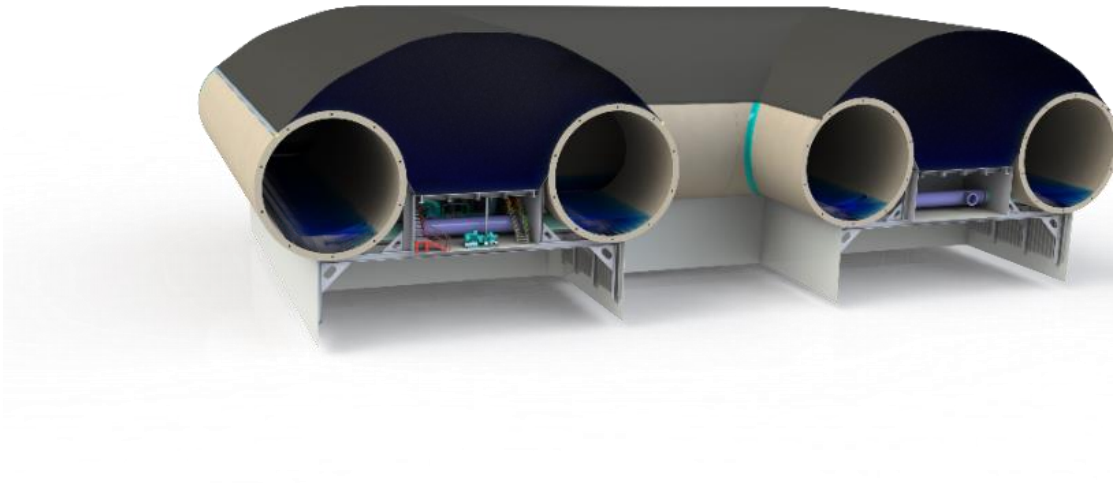

Figure 2: Overview of the OB with the tubes as rigid reservoirs and a flexible storage bladder on top (van Rooij, 2020).

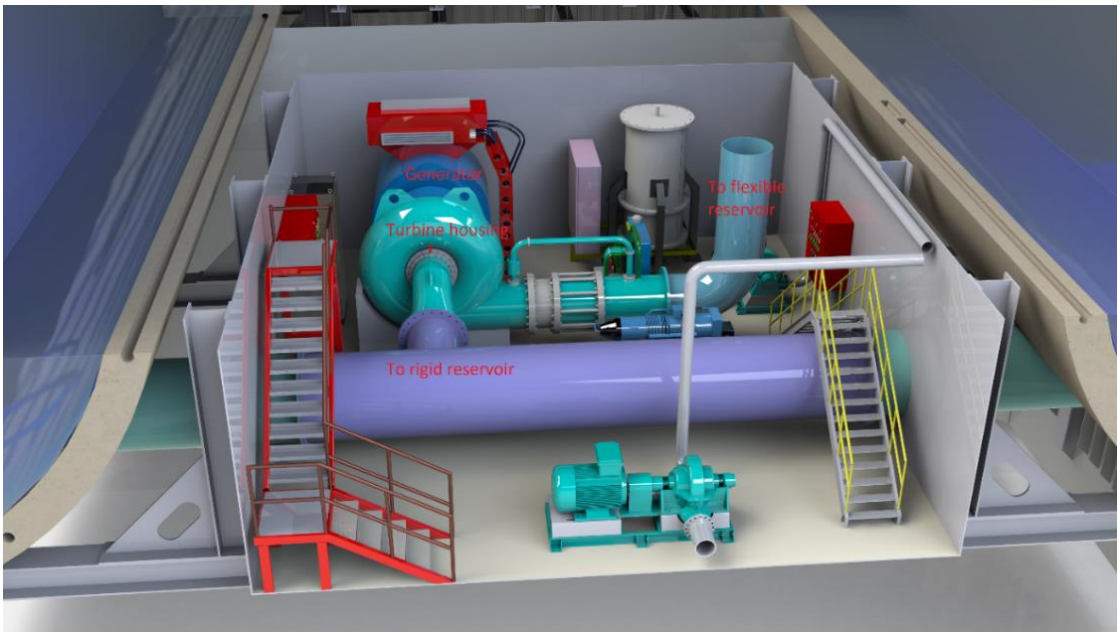

Figure 3: Detailed overview of the OB working principle, the purple pipe is connected to the rigid reservoirs, the blue pipe behind it, is connected to the flexible reservoir. The two pipes are also connected, and a reversible turbine is present to pump water into the flexible reservoir or supply energy to the generator behind it (van Rooij, 2020).

3. Problem owner & Stakeholders analysis

The problem owner in this research is Marijn van Rooij, the Chief Technical Officer of OG. He is responsible for all the technical components of the Ocean Grazer 3.0 and that they function optimally. Van Rooij is uncertain whether the current electricity connection between the WEC and the Ocean Battery considered is optimal. Therefore, he would like to investigate the efficiency of a hydraulic system connecting the WEC and the Ocean Battery. As this is a technical problem for Ocean Grazer, he is the problem owner.

Additionally, Wout Prins, founder of the Ocean Grazer is a stakeholder. Prins wants to realize a competitive product on the energy market. Therefore, the Ocean Grazer system must be as efficient as possible. As it is uncertain that this is the case currently, he is interested in the efficiency of a hydraulic system to improve the overall efficiency of the Ocean Grazer 3.0.

Furthermore, prof. dr. Antonis Vakis is considered a stakeholder as supervisor of this project. Additionally, as the co-founder and scientific advisor, he is interested in the output of this research as that could provide further research possibilities for the final implementation of a more efficient system to connect the WEC and the Ocean Battery.

4. Problem analysis & statement

In the current concept, wave energy is harvested by a WEC in the form of mechanical energy. The mechanical power is thereafter converted to electricity. Consequently, the electricity is transported to the Ocean Battery. In the Ocean Battery, the electricity can be converted to mechanical power to charge the Ocean Battery. Ocean Grazer is uncertain whether converting the harvested mechanical energy to electricity is the most efficient way to charge the Ocean Battery. The current concept is depicted in Figure 4.

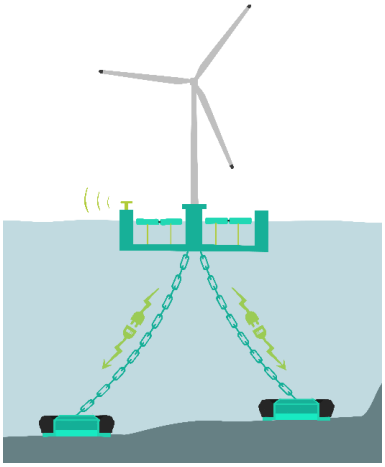

Figure 4: Schematic overview of the current electrical concept of Ocean Grazer (van Rooij, 2020).

It could be more efficient when mechanical energy that is harvested from waves is converted to fluid power. In that case, a high-pressure hydraulic tube must connect the WEC with the OB to transport the fluid power to a hydraulic motor that converts the fluid power back to mechanical power. Consequently, the Ocean Battery can be charged with a pump, or electricity could be generated by a generator. Such a hydraulic system may be more efficient than an electrical system. Therefore, OG would like to know the efficiency of such a hydraulic system. The problem can be defined as follows:

'Ocean Grazer Holding B.V. is uncertain about the efficiency of a hydraulic system connecting the Wave Energy Converter and the Ocean Battery.'

5. System description & Scope

Now that the problem is defined, the system is described. The WEC harvests mechanical energy from the waves. The mechanical energy must be converted to fluid power by a power take-off system (PTO). Currently, a new PTO is being designed by Jeffin Jacobs, a master student performing research for Ocean Grazer. The WEC and PTO are therefore out of the scope in this research. After the conversion to fluid power, it must be transported through a hydraulic tube to the OB. This is to be done by hydraulic fluid under high-pressure. High-pressure is used such that the radius of the tube does not need to be too wide. Since the hydraulic tube is to be in the sea, it is

on one hand more favourable to have a relatively small radius as this increases the flexibility. On the other hand, a larger radius would be favourable as the losses in the tube decrease for larger radii. Therefore, a compromise is to be determined between these two aspects.

At the Ocean Battery, the hydraulic fluid utilized must deliver the fluid power to a hydraulic motor. The hydraulic motor must convert the fluid power back to mechanical power. The motor utilizes the pressure difference across the inlet and outlet of the fluid to translate the fluid power into mechanical power. The mechanical power is then supplied in the form of torque and angular velocity to the output shafts. One of these shafts must be connected to a pump or PAT, the other output shaft to a generator. After passing through the motor, the hydraulic fluid is transported back under a lower pressure to the ocean surface, where it must be reused.

With a pump or a PAT, water can be pumped from the rigid reservoirs into the flexible bladder to store potential energy. With a PAT, the stored potential energy can be discharged through the same machine, and no extra turbine is necessary. If a pump were to be implemented, a separate turbine would also be necessary to discharge the water in the flexible bladder to drive a generator. Ocean Grazer is not certain yet, whether it will use a separate pump and turbine or a PAT because no research has been performed yet on PATs. Finally, the generator can generate electricity through the mechanical power delivered by the hydraulic motor, the turbine or the PAT. Thereafter, this electricity can be transported to consumers.

As research is currently being done on a new power take-off device, the conversion of mechanical energy to fluid power in the WEC at the ocean surface is left out of the scope. The WEC and the placing of the hydraulic motor in the OB are out of the scope as well. Furthermore, it is assumed that the tubes act like rigid pipes, with a length of 70 meters whereas realistically they must be flexible due to the forces of the ocean currents. 70 meters is used because the OB is expected to be stationary at a depth of 100 meters and the PTO supplying the fluid power will be at a depth of 30 meters.

In conclusion, the system that is described consists of two parts. In this research only the latter part will be investigated. The following aspects are focussed on in this research. The hydraulic motor, the hydraulic tube system as well as a hydraulic fluid were modelled. Furthermore, a literature survey on PATs and generators is delivered. It must be noted that the hydraulic fluid depends on the hydraulic motor as the motor must be able to function with the type of fluid. Additionally, the hydraulic motor must supply torque and angular velocity to a pump or PAT and be able to deliver this to a generator as well. Finally, the radius of the hydraulic tubes must also be determined. In Figure 5 a schematic overview of the scope considered in this research is depicted.

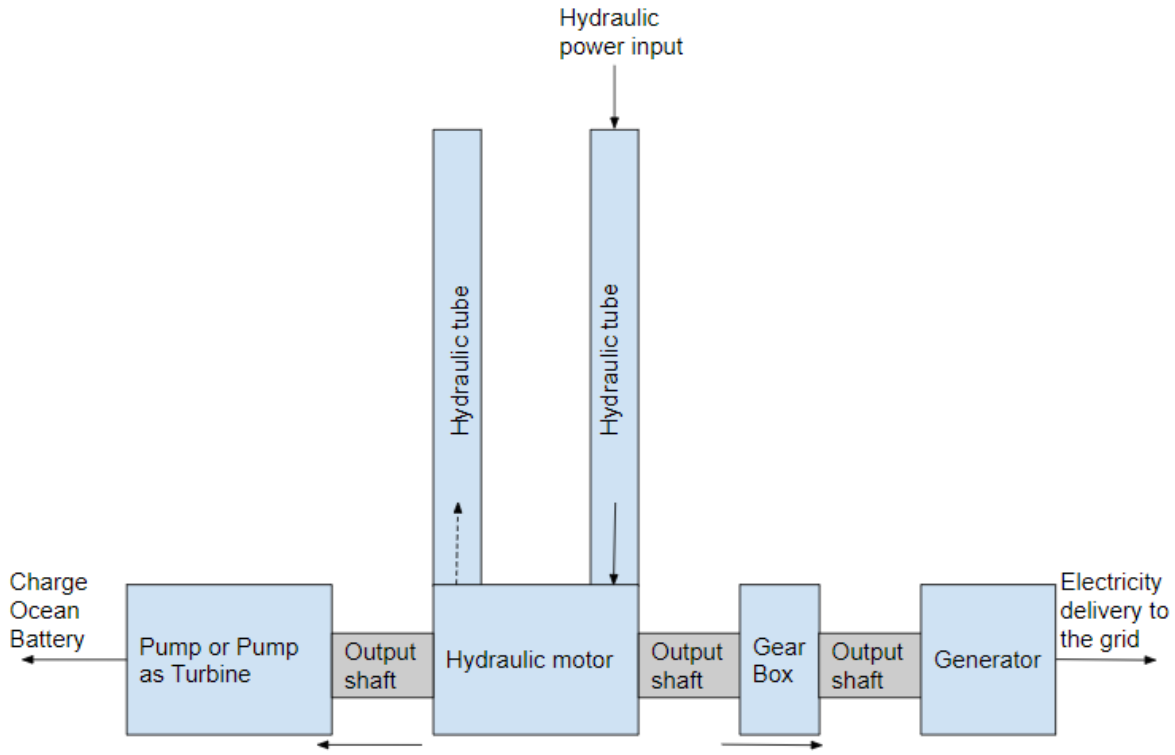

Figure 5: Schematic overview of the scope considered in this paper. The arrows show the energy flow through the system. The power delivered to the hydraulic motor can either be directed to the generator or the pump. It must be noted that the pump or PAT must also be able to supply energy to the generator. The dotted arrow shows the fluid flow back to the PTO. The need for a gearbox is verified in chapter 11.

6. Research objective

It must be determined which hydraulic motor, hydraulic fluid, the radius of the high-pressure tube, generator, and PAT can be combined to determine the conversion efficiency of the scoped system. The components each have their properties, and a model can be used for calculations of the conversion efficiency of the system described. By simulating the model, the losses in the scoped system can be computed. Therefore, the research objective is phrased as follows:

'To obtain a design of the scoped system by combining a hydraulic motor, hydraulic fluid, radius of the hydraulic tubes and a generator and use the physical properties of these components to determine the losses and conversion efficiency in the scoped system, all within 3 months.'

7. Research questions

To realize the goal, the following research questions must be answered to obtain a design of the scoped system to compute the efficiency. By finding and modelling the functional components, the efficiency of the hydraulic system can be obtained analytically.

- What is the conversion efficiency of the scoped system?
    - Which hydraulic motor is applicable in the system?
    - Which PAT is applicable in the system?
    - Which generator is to be used in the system?
    - What is the conversion efficiency of this motor in the system?
    - Which hydraulic fluid is optimal in the system with the selected hydraulic motor?
    - What is the radius of the high-pressure hydraulic tube?
    - What are the total losses in the scoped system?

8. Methods and tools

As this is the first research regarding the described system, this research consists of two parts. In the first part, a survey of components that could be utilized is outlined. Ocean Grazer has indicated that they have little information about generators, hydraulic motors and the advantages and disadvantages of using PATs. Therefore, knowledge is provided in this research about these components such that a basis is provided for the definite selection of the specific machines.

The second part will be simulating a model of the hydraulic system described. For the simulations, Simulink is utilized. Simulink is a programme created by MathWorks. Within Simulink, there is a useful add-on called Simscape. It is utilized because it already has several built-in features for hydraulic, mechanic and electric systems and energy loss computations.

9. Hydraulic motors

Firstly, the hydraulic motor is investigated. There are three main categories of hydraulic motors. Namely, gear motors, vane motors and piston motors. The first two are not suitable for high-pressure use and are therefore not discussed in this research (Chapple, 2015). Therefore, a piston motor must be selected to deliver mechanical power to the generator and the PAT. Two types of piston motors can be distinguished: axial piston motors and radial piston motors. In the next section, their properties and functions will be discussed.

9.1. Axial piston motor

In axial piston motors, fluid pressure pushes against the pistons. The variety of pressure per piston causes the pistons to slide around a swashplate. Because the swashplate is inclined at an angle and connected to a cylinder, the swashplate and cylinder start to rotate due to the movement of the pistons. An example of an axial piston motor is depicted in Figure 6.

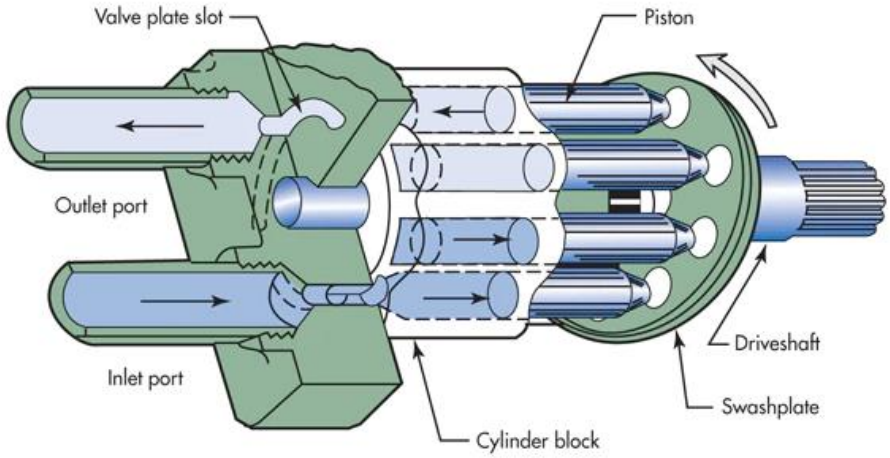

Figure 6: Axial piston motor (Hydraulics & Pneumatics, 2014).

Axial piston motors are used for low torque and high angular velocity operations. A gearbox is not always necessary for axial piston motors due to their high angular velocity which is an advantage (Chapple, 2015) (Hydraulics & Pneumatics, 2014). However, no axial piston motor was determined from the literature that could function with the flow rate that is determined in chapter 14.

9.2. Radial piston motor

A radial piston motor consists of multiple pistons which are carried in a cylinder block. This cylinder block is mounted on a driveshaft, which incorporates an offset from the centre of rotation. Hydraulic fluid under high pressure can be fed to each piston through fluid paths in the crankshaft of the motor. Pressurizing the pistons in combination with the offset driveshaft creates a turning motion. This turning motion

creates mechanical power, which can drive other machinery.

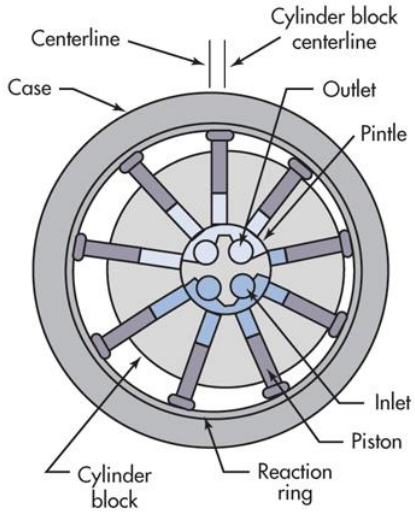

Figure 7: Radial piston motor (Hydraulics & Pneumatics, 2014).

Radial piston motors are used for high torque and low angular velocity applications (Chapple, 2015) (Hydraulics & Pneumatics, 2014) (Rotary Power, 2018). In figure 7, an example of a radial piston motor is illustrated.

From Bosch Rexroth, one of the major hydraulic motor suppliers in the Netherlands, it was obtained that the flow rates allowed by axial piston motors were limited and therefore the axial piston motors were inadequate. Whereas there were several suitable radial piston motors (Bosch Rexroth, 2019). Therefore, for the simulation, a radial piston motor is utilized.

Specifically, the technical data of the CBM 3000 2200 8 port by Hägglunds is utilized for the simulations (Bosch Rexroth, 2012) (Bosch Rexroth, 2019). This is a fixed displacement motor. This motor has the desired specifications such that it can function with the given flow rate and pressure.

10. Pump as Turbine

Next, the possibilities of using PATs in the Ocean Battery are explored. In the simulation of the energy flow in the Ocean Battery presented before, a pump model and a turbine model for calculations of the efficiency in the Ocean Battery were established (van Kessel, 2020). This might suggest the use of a separate pump and turbine. However, it was indicated by Marijn van Rooij that Ocean Grazer would like to investigate the use of a or several PATs instead of a separate pump and turbine. This is because PATs have several advantages over the use of a separate pump and turbine. Additionally, PATs are frequently used in smaller hydropower plants such as the Ocean Grazer concept (Binama, et al., 2017).

First, the working principle of PATs is explained. PATs are reversible pumps. This entails that PATs can both pump fluids as well as function as a turbine and generate mechanical energy. In figure 8, different types of PATs and their applications ranges are depicted. Based on the head and flow rate required, Ocean Grazer can determine which type of PAT could be implemented in the Ocean Battery once the company is certain about the use of PATs.

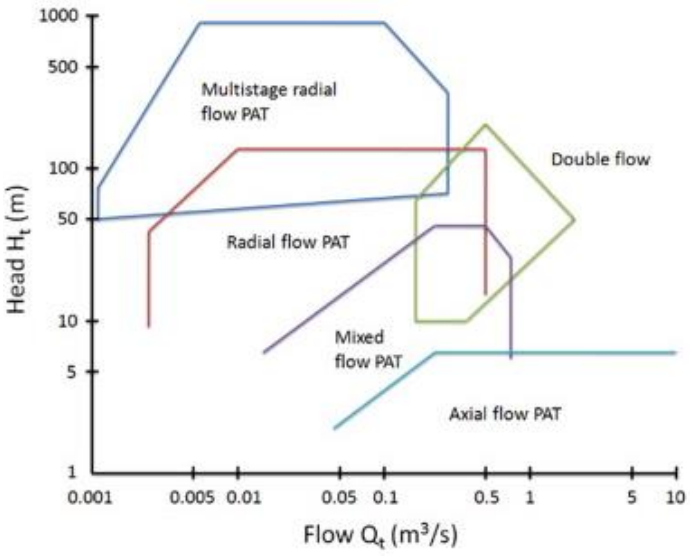

Figure 8: Different pump types suitable as turbines (Jain & Patel, 2014).

The next section will elaborate on the advantages and disadvantages of the use of PATs in the Ocean Battery to provide Ocean Grazer with information regarding PATs. The first advantage that is indicated, are the costs of a PAT over a conventional pump and turbine. Especially conventional turbines have a record of being very expensive to purchase and often pay back their purchase costs only after 15 years (Budris, 2011). Whereas for a PAT this period can be as short as 2 years.

Furthermore, PATs are more reliable than turbines. Due to the simple design of pumps, they do not require much maintenance and they have little failures. Moreover, they have a long-life cycle and are relatively easy to operate and maintain. This property of PATs could be extremely valuable for Ocean Grazer, as maintenance

costs are expected to be high because the Ocean Battery will be offshore and on the bottom of the sea.

The last major advantages are the availability of PATs for a wide range of heads and flows, the short delivery time, ease of finding spare parts for maintenance and easy installation. This is because pump technology is much simpler and more mature than conventional hydro turbine technology.

PATs also have various limitations. The first limitation of PATs is the selection of the type of PAT for a specific site. This is because manufacturers provide information about the performance of PATs in pumping mode, however, they do not supply information regarding the turbine mode performance of PATs. Many researchers have developed methods to theoretically or experimentally determine the performance of PATs in turbine mode, however, there are still limitations in these methods.

Furthermore, PATs have a relatively small operating range. Whereas conventional turbines reach high efficiencies over a wide operating range, PATs only reach a high efficiency from 80% to 100% of the operating range (Jain & Patel, 2014) Therefore, for fluctuating power inputs of PATs, it is advised to utilize several PATs in parallel. This is because in that case, a wider range of higher efficiencies can be obtained, which is visible in figure 10 below (Carravetta, et al., 2018). It is important for OG, to keep this in mind when decisions are made regarding the implementation and selection of a PAT.

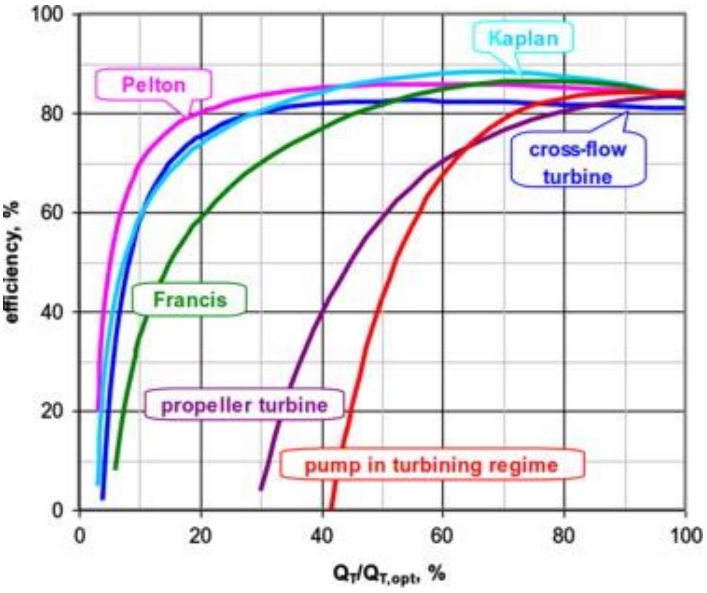

Figure 9: Operating range of PATs in turbine mode (Jain & Patel, 2014).

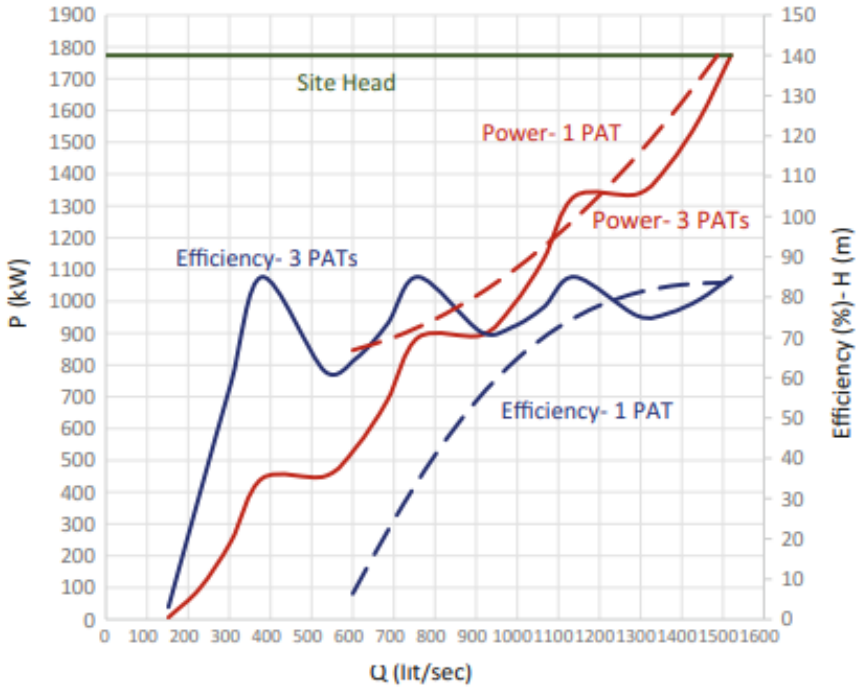

Figure 10: Efficiency of three parallel PATs vs one large PAT (Carravetta, et al., 2018).

Another disadvantage of PATs is that the efficiency of PATs is generally lower than the efficiency of conventional hydro turbines. However, this is certainly not the only criterion for the decision to implement PATs (Jain & Patel, 2014) (Carravetta, et al., 2018).

Furthermore, in the paper presented by Barbarelli, 12 PATs are tested in pump mode as well as in reverse mode, as a turbine (Barbarelli, et al., 2017). The 12 pumps are experimentally tested in a test rig. The experimental setup and results could be useful to review for Ocean Grazer if the company decides to implement PATs.

11. Generators

The following section will elaborate on types of generators that could be utilized to convert the mechanical energy delivered by the turbines or the hydraulic motor to electricity. It is determined which types of generators could be utilized, and why they do or why they do not present a feasible option to generate electricity in the Ocean Battery. It was indicated that generator research was limited by Ocean Grazer. A commencement for further research for the final selection of the optimal generator to be implemented in the Ocean Battery is provided because little quantitative data was found, and no testing could take place. Therefore, it was not possible to select a definite optimal generator for the system. However, an outline of the possibilities is provided and qualitative reasoning for a recommendation is utilized.

Windmill generators have been studied for the selection of a generator type because just like this system, wind turbines also generate variable power, because of changes in the wind speed. Selection criteria are provided later in this chapter, to determine a preliminary optimal type of generator.

The basic working principle of generators is as follows. Generators consist of a stator and a rotor. Due to the poles in the rotor and three-phase windings in the stator, a rotating magnetic field is created. The rotating magnetic field causes current to flow through the coils. The current can be delivered to an electricity grid.

11.1. Criteria

Next, several criteria for generators are outlined. These criteria include reliability, efficiency, maturity, maintenance costs, purchase costs, controllability and coping with variable angular velocity inputs. Since no quantitative comparable data was found, the generator recommended in this report will be based on qualitative reasoning and discussion with the stakeholders about the importance of the criteria.

Firstly, a brief explanation of the criteria. Reliability is defined as the frequency and duration of failures. The efficiency is the ratio between energy output and energy input. The efficiency changes depending on the load exerted on the generator rotor. Maturity is defined as the extent to which the generator is utilized in offshore wind energy since wind energy power plants show characteristic similarities with the Ocean Battery. From the market share illustrated in figure 11, the maturity of types of generators can be derived.

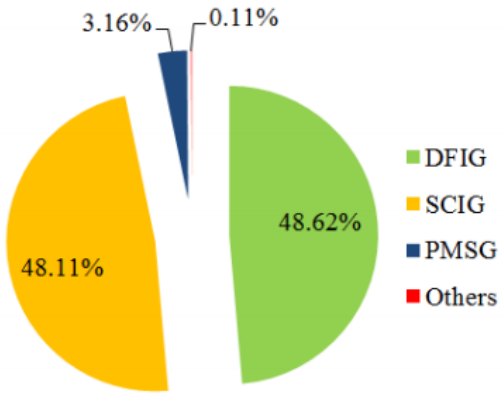

Figure 11: Market share of current generators used in offshore wind energy generation (Zhang, et al., 2013).

Furthermore, maintenance costs are the costs to fix failures. Purchase costs are the costs associated with the acquisition of the machine. Controllability is defined as the complexity to stay in the appropriate angular velocity range, to prevent failures. Control systems aim to maximize power output. Generators need to be controlled to avoid rotation above the maximum angular velocity because that damages the generator. Furthermore, if the control is very complex, the generator is more complex to operate and the control system is also more expensive, both lead to extra costs. Lastly, coping with variable angular velocity input usually is a criterion. However, since the angular velocity delivered by the hydraulic motor is constant, it is not certain at this point that this criterion is relevant. The relevance of this criterion depends on the turbine or PAT that will be implemented, which is uncertain at the time of writing.

It is important to note that not all the criteria are exclusive of one another. Therefore, when selecting a definite generator type, this should be considered in the assessment. There are connections between reliability and maintenance costs. For example, if the reliability of a generator is very high, the maintenance costs are lower than in the case where frequent failures of the generator occur. Additionally, there is a connection between maturity and controllability. Mature generators have mature control systems and are therefore simpler to control.

11.2. Generator types

Two types of generators are distinguished: induction generators and synchronous generators. Both use the same working principle; however, the synchronous generator rotates at the synchronous angular velocity whereas the induction generator must rotate at an angular velocity that is higher than the synchronous angular velocity to generate electricity (Circuit Globe, 2018). That is why the induction generator is also called an asynchronous generator.

Furthermore, the synchronous angular velocity of a generator can be determined with the following formula (Circuit Globe, 2018):

$$N = \frac{120 f_e}{P_n} \quad (1)$$

where N is the synchronous angular velocity of the generator in rpm, f_e is the frequency of the electricity grid and P_n is the number of poles in the generator. Therefore, the more poles there are in a generator the lower the angular velocity. Naturally, poles come in pairs and therefore only even number of poles are allowed. The synchronous angular velocities for generators with 2 to 20 poles are displayed in Table 1:

Pole number	Synchronous angular velocity in rpm (50 Hz)	Synchronous angular velocity in rpm (60 Hz)
2	3000	3600
4	1500	1800
6	1000	1200
8	750	900
10	600	720
12	500	600
14	428.6	514.3
16	375	450
18	333.3	400
20	300	360

Table 1: Synchronous generator angular velocities corresponding to the number of poles.

Generally, generators do not have more than 20 poles, since generators will then become enormous and expensive. In wind energy power generation, generally, 4 or 6 pole generators are utilized (Danish Wind Industry Association, 2003). Additionally, with table 1 it is possible to conclude that the system certainly needs a gearbox because the angular input velocity of the generator is higher than the maximum angular velocity of 29 rpm of the hydraulic motor.

It is advised to test generators under similar conditions as they will be used in before they are implemented in a system. This is because generally manufacturers and operators provide little quantitative data on the performance of generators. However, since testing is currently not possible due to the coronavirus and the costs of the different types of generators, the main qualities of each generator are described here from literature.

The types of suitable generators and their characteristics presented in the next sections, are based on (Alnasir & Kazerani, 2013) (Hansen, et al., 2001) (Baroudi, et al., 2007) (Electropaedia, sd) (Ra, et al., 2015) (Esterhuizen, 2019).

11.2.1. Induction generators

Based on the rotor type, induction generators can be divided into two categories. The squirrel cage induction generator (SCIG) and the wound-rotor induction generator (WRIG). Furthermore, induction generators need to be continuously excited by a

source of reactive power to generate a voltage and active power. In figure 12 a generalized torque speed curve of induction machines is illustrated. As displayed, induction generators function as motors for lower angular velocities. To generate electricity, the angular velocity must be higher than the synchronous angular velocity. For every induction generator, there is an angular velocity for maximum efficiency. This is at point M in figure 12. Notice that the 'pushover torque' is generating torque, which is opposite to the movement of the rotor.

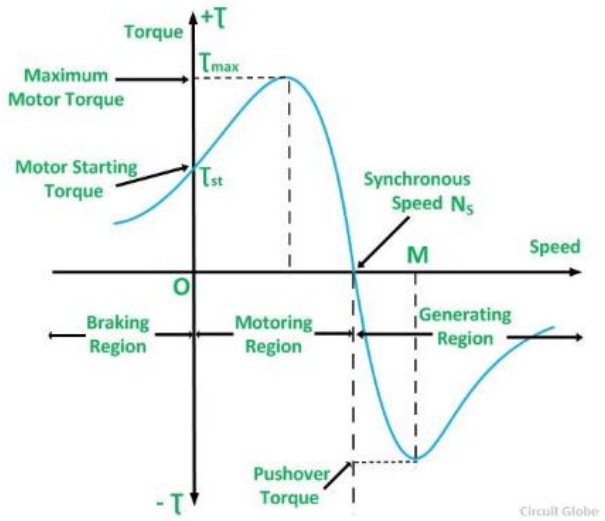

Figure 12: Characteristic torque speed curve of induction machines. The machine is started as a motor, for angular velocity higher than the synchronous angular velocity the machine starts generating electricity. Point M indicates the point of maximum efficiency (Circuit Globe, 2018).

Squirrel Cage Induction Generator

The rotor of the Squirrel Cage Induction Generator (SCIG) consists of short-circuited conduction bars that are shaped like a squirrel cage. The conventional squirrel cage induction generator is a mature and the most reliable design. It is economical, relatively simple and small due to the little components. However, this comes with lower efficiency, as can be observed in Figure 13, due to the full capacity power converters required. The power converters must deliver magnetizing current as reactive power.

Permanent Magnet Induction Generator

The Permanent Magnet Induction Generator (PMIG) is much alike the SCIG. However, the SCIG suffers from low efficiency due to power converters, whereas a PMIG can partially supply a magnetic flux to reduce the magnetizing current required by the conventional SCIG. This can be achieved by placing a permanent magnet rotor inside the squirrel cage rotor. The outer SC rotor is connected to the rotating input shaft and is excited from the PM rotor because the PM rotor is free to rotate against the shaft. PMIGs have the advantages that they have high efficiency, as shown in Figure 13, and are generally reliable. However, it is also more complex in construction and the magnets are expensive. Furthermore, the availability of permanent magnets

is unclear in the future due to limited suppliers, mostly from China, and the impact of politics on the stability of the market.

Wound-Rotor Induction Generator

The rotor of the wound-rotor induction generator (WRIG) contains a three-phase winding like its stator. The rotor can be connected to a set of slip rings and brushes or a power electronic converter can be utilized to excite the rotor. The advantage is that it is simply controlled. The limited angular velocity range, purchase costs, reduced lifetime and reduced efficiency are the drawbacks of this system.

Doubly Fed Induction Generator

The doubly-fed induction generator (DFIG) is a version of the WRIG where the rotor is also connected in a bidirectional way to the electricity grid. The rotor angular velocity can be adjusted by either taking power from the grid to increase the angular velocity or deliver power to the grid to reduce the angular velocity. This means that either power can be taken from the generator to the grid or the other way around. The advantages include high efficiency, as depicted in Figure 13, mature design and therefore mature control systems. However, due to the usage of brushes and slip rings, extra maintenance is required.

Brushless Doubly Fed Induction Generator

The brushless doubly-fed induction generator (BDFIG) has two stator windings with a different number of poles in the stator, one for generation and the other one for control. It is comparable to the DFIG; however, it is larger, more expensive and more complex to control, furthermore it is a new type of machinery that is not available on the commercial market yet. However, in the future, it could be attractive for offshore applications since less maintenance is required since no brushes and slip rings are required.

11.2.2. Synchronous generators

Synchronous generators generally have an advantage over induction generators that it is possible to eliminate the need for a gearbox. This reduces maintenance requirements and increases system reliability and efficiency. However, this appears impossible since the hydraulic motor has a relatively low angular velocity output. The synchronous generator current output depends directly on the torque provided by the hydraulic motor through the gearbox.

The stator of synchronous generators is essentially the same as for induction generators, however, the rotor can either be cylindrical or use salient poles. Two types are distinguished: the wound rotor synchronous generator (WRSG) and the permanent magnet synchronous generator (PMSG).

Wound Rotor Synchronous Generator

The WRSG has essentially the same characteristics as the WRIG, however, the WRSG must be excited by a DC source. To excite the rotor winding, brushes and slip rings or a brushless excitation system must be included. This features higher complexity and maintenance costs which are the main obstacles for adopting WRSG. Also, for

variable angular velocities, a full power inverter is required, which reduces efficiency. Lastly, the efficiency is rather limited for partial loads as demonstrated in Figure 13.

Permanent Magnet Synchronous Generator

The PMSG is a self-excited brushless synchronous generator. It has similar characteristics to the PMIG. Again, the magnets are costly, and the supply is uncertain in the future. However, the machine has high efficiency as demonstrated in figure 13 and is generally reliable. Lastly, the drawback is that the availability of permanent magnets is unclear in the future.

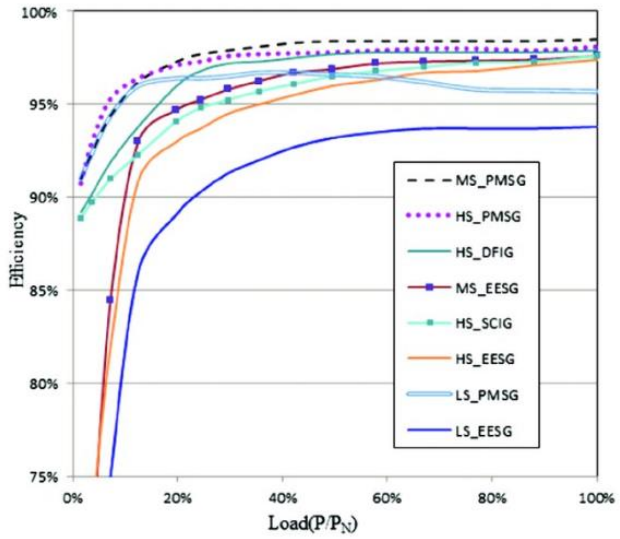

Figure 13: Efficiency vs load curve, for low, medium and high wind speeds, of the PMSG, DFIG, SCIG and WRSG (EESG in the graph) (Thirumalai & Chenniappan, 2017).

Lastly, an overview of the advantages and disadvantages per generator type is provided in table 2.

Generator	**Advantages**	**Disadvantages**
Squirrel Cage Induction Generator	Simple, most reliable, easy control, mature machine, relatively cheap	Low efficiency
Doubly Fed Induction Generator	High efficiency, easy control, mature technology	Brushes and slip rings require maintenance.
Permanent Magnet Synchronous Generator	High efficiency, reliable	Magnet cost, complex control, magnet supply dependent on China, a relatively new machine
Brushless Doubly Fed Induction Generator	High efficiency, high reliability	Complex control, very new machine
Wound Rotor Induction Generator	Easy control	Limited operating range, low efficiency, low reliability

Wound Rotor Synchronous Generator		Low reliability or high control complexity, unpredictable efficiency
Permanent Magnet Induction Generator	High efficiency, reliable	A relatively new machine, magnet costs, magnet supply dependent on china, complex control

Table 2: Overview of the types of generators and their advantages and disadvantages.

11.3. Generator recommendation

From the generator types described, it must be derived which one(s) are most suitable for further research to determine an optimal generator for Ocean Grazer. The criteria were discussed with the problem owner, Marijn van Rooij, and Wout Prins, it was determined that reliability, efficiency and maturity were the most important criteria. Purchase costs, maintenance costs and controllability were considered less important criteria. Because the importance of coping with variable angular velocity input is uncertain at this point, it was not considered in this recommendation.

Because of the high reliability, the maturity, the simple controllability and the low purchase costs of the Squirrel Cage Induction Generator, this type is recommended for the Ocean Grazer system. The SCIG is the most reliable and together with the DFIG the most mature in the offshore wind industry. Therefore, it is also relatively simple to control. Furthermore, it can be derived from Figure 13 that the efficiency is only slightly lower in high angular velocity operation than that of the other types of generators in Figure 13.

Alternatively, the DFIG could be implemented. The DFIG has a higher efficiency than the SCIG. However, it is less reliable and therefore it should be determined how often maintenance in the Ocean Battery will take place. If the DFIG breaks down much more frequent than the other components in the Ocean Battery, it should not be utilized. However, if maintenance will frequently take place anyway in the Ocean Battery due to other machinery breaking down, the DFIG could also be an option for Ocean Grazer.

Lastly, as it is yet uncertain when the Ocean Grazer concept will be ready for application on a commercial scale, in the future the BDFIG could also present a suitable option to function in the Ocean Battery. This new technique also has the advantage of being very reliable and it has a higher efficiency than the SCIG. However, this machine is still in a developing stage and is not commercially applicable due to its high costs at the time of writing.

12. Modelling energy losses

To model the scoped system described, Simulink is used. The libraries in Simulink contain Simscape, which is utilized to create a model of the part of the system researched in this report. Simscape is a part of Simulink, it can be used to model multi-domain physical systems. Simscape will be used since it includes models of hydraulic motors, tubes, and generators to calculate the energy losses in such components. Therefore, this program will be utilized for the energy losses computations of the system researched in this report. Moreover, it is possible to adjust the parameters needed swiftly. For an overview of the model in Simscape, see Appendix I. In the description of the model and the simulation, a steady-state is referring to the behaviour of the system after the time it takes to start the motor.

12.1. Power inputs

The hydraulic power input, P_H, is a function of the pressure input, p_{in}, and the flow rate, q.

$$P_H = p_{in} q \tag{2}$$

To obtain the fluctuating power input, a variable pressure source was utilized in Simscape. The pressure input is a function of time, t.

$$p_{in} = f(t) \tag{3}$$

The pressure source is the input of the system. The pressure input is generated with a sine wave to obtain a variable pressure input. The input pressure is specified as:

$$p_{in} = p_m + p_d \sin\left(-f_w(t + \varphi)\right) \tag{4}$$

where p_m is the mean input pressure, p_d is the pressure difference between the extreme pressure inputs and the mean input pressure, f_w is the frequency of the sine wave and φ is the phase shift.

12.2. Hydraulic Resistive Tube

Firstly, the generated input travels through a hydraulic tube. The hydraulic resistive tube block in Simscape (MathWorks, 2009) can be used to model circular pipelines both rigid and flexible. Friction losses in the tube can be computed to determine the energy losses. For laminar flow, the flow rate is proportional to the pressure gradient. Whereas for turbulent flow, the flow rate is proportional to the square root of the pressure gradient. In both cases, the flow rate is a function of the pressure loss over the tube, Δp.

$$q = f(\Delta p) \tag{5}$$

This is because both the flow rate and the pressure difference are a function of the average velocity of the fluid. Therefore, the flow rate can also be expressed as a function of the hydraulic diameter of the tube, D_H, and the average velocity of the fluid through the tube, v, as follows.

$$q = \frac{\pi D_H^2}{4} v \tag{6}$$

Pressure loss due to friction in the tube is computed using the Darcy equation. The pressure loss in this equation is a function of the friction factor, f, the length of the tube, L, the density of the fluid, ρ, and the square of the average velocity of the fluid over twice the diameter of the tube. The Darcy equation reads as follows:

$$\Delta p = \frac{f L \rho v^2}{2 D_H} \tag{7}$$

As shown in the Darcy equation, the pressure loss is computed with the friction factor. The friction factor depends on the type of flow through a tube. The flow through tubes can be either laminar or turbulent. For turbulent flow ($Re \geq 4000$), the Haaland approximation is utilized to determine the friction factor. In Simscape, the friction factor in the transitional phase is computed by linear interpolation between extreme points of the laminar and turbulent flow. For laminar flow ($Re \leq 2000$), the friction factor is calculated by dividing the shape factor by Reynold's number, Re. The shape factor is 64 in the case of a circular tube.

$$f = \frac{64}{Re} \quad for\ Re \leq Re_L \tag{8}$$

$$f = f_L + \frac{f_T - f_L}{Re_T - Re_L}(Re - Re_L) \quad for\ Re_L < Re < Re_T \tag{9}$$

$$f = \left(-1.8 log_{10} \left(\frac{6.9}{Re} + \left(\frac{\frac{r}{D_H}}{3.7} \right)^{1.11} \right) \right)^{-2} \quad for\ Re \geq Re_T \tag{10}$$

where Re_L is the maximum Reynolds number at laminar flow, Re_T is the minimum Reynolds number at turbulent flow, f_L is the friction factor at the laminar border and f_T is the friction factor at the turbulent border. The friction factor for critical flow, $Re_L < Re < Re_T$, is computed by linear interpolation between extreme points of the flow regime by Simscape. Lastly, r is the roughness of the internal surface of the hydraulic tube.

Furthermore, Reynold's number is a function of the fluid's velocity, the diameter of the tube and the kinematic viscosity of the fluid. It is expressed accordingly:

$$Re = \frac{v D_H}{\nu} \tag{11}$$

In the model, only one hydraulic resistive tube will be utilized. The tube to transport the fluid to the hydraulic motor. For the energy loss from power input to the power output of the system, the influence of the hydraulic tube to transport the fluid back to the reservoir in the WEC is minimal. This is because the hydraulic motor uses the pressure difference over the inlet and outlet of the hydraulic motor. Therefore, the exact value of the inputs and outputs is irrelevant for hydraulic motor behaviour. Furthermore, manufacturers can customize the output pressure to the requirements of the user, whereas this could not be indicated in Simscape. Since the changes in the

hydraulic tube pressure loss are very small for a large difference of input pressures, as will be demonstrated in chapter 14, and the limitations of Simscape to set a constant output pressure of the hydraulic motor, the extra pressure loss in the hydraulic tube due to a slightly higher input pressure, in reality, is ignored.

12.3. Hydraulic fluid

The hydraulic fluid block in Simscape (MathWorks, 2006) can be utilized for simulations of the fluid in the hydraulic system. Simscape has several standard fluids and their properties that are frequently adopted by users of Simscape in hydraulic systems. The hydraulic fluid must be able to operate in the hydraulic motor that will be utilized in the model. The hydraulic motor used in this research can function with multiple hydraulic fluids. One group of fluids that can be used are HFD synthetic esters. HFD synthetic esters are fluids that are fire-resistant and do not contain water (Quaker Chemical Corporation, 2020). One of the standard fluids in Simscape is Fluid MIL-F-83282. This fluid is such an HFD synthetic ester. Therefore, this fluid will be utilized in the simulations.

12.4. Hydraulic motor

Simscape contains a fixed displacement hydraulic motor (MathWorks, 2006), which will be utilized to simulate the model. With the fixed displacement motor, the energy losses in the motor can be determined. There are two different types of losses considered in the motor: volumetric losses due to leakage and mechanical losses due to torque friction. Now it is demonstrated how the energy losses due to leakage and friction can be computed.

The volumetric flow rate to power the motor is given by:

$$q = q_{ideal} + q_{leak} \tag{12}$$

where q_{ideal} is the ideal volumetric flow rate without leakage and q_{leak} is the internal leakage volumetric flow rate. The maximum flow rate through the hydraulic motor can also be determined, such that this value will never be exceeded.

$$q_{max} = D\omega_{max} \tag{13}$$

Furthermore, the relation between the ideal flow rate, without leakage, and the ideal angular velocity is determined by:

$$\omega_{ideal} = \frac{60 q_{ideal}}{D} \tag{14}$$

where D is the displacement per revolution of the hydraulic motor and ω_{ideal} is the angular velocity of the output shaft corresponding to the ideal flow rate. The angular velocity in rpm is divided by 60 to convert revolutions per minute to revolutions per second. Furthermore, the internal leakage flow rate is a function of the Hagen Poiseuille coefficient for laminar pipe flow, K_{HP} and the pressure drop over the motor, Δp_m.

$$q_{leak} = K_{HP}\Delta p_m \tag{15}$$

The Hagen Poiseuille coefficient is determined as follows:

$$K_{HP} = \frac{\nu_{nom}\rho_{nom}\omega_{nom}D}{\rho\nu\Delta p_{nom}}\left(\frac{1}{\eta_v} - 1\right) \tag{16}$$

where ν_{nom} is the nominal kinematic viscosity of the hydraulic fluid, ρ_{nom} is the nominal density of the fluid, ω_{nom} is the nominal shaft angular velocity, ρ is the actual density of the hydraulic fluid, ν is the kinematic viscosity of the hydraulic fluid, Δp_{nom} is the nominal pressure drop, η_v is the volumetric efficiency relating to the nominal conditions. These nominal values are the values at which the volumetric efficiency is specified.

Next, the losses due to friction in the motor are explained. First, the torque generated by the motor is computed as follows:

$$T = T_{ideal} - T_{friction} \tag{17}$$

where T is the torque generated by the motor, T_{ideal} is the ideal torque, without friction, produced by the motor and $T_{friction}$ is the torque loss due to friction.

The ideal torque generated can be determined in the following manner:

$$T_{ideal} = D\Delta p_m \tag{18}$$

To compute the friction loss in the motor, the torque loss due to friction must be computed:

$$T_{friction} = (T_0 + K_{TP}|\Delta p_m|)\tanh\left(\frac{4\omega_{ideal}}{\omega_{threshold}}\right) \tag{19}$$

in which T_0 is the no-load torque. This is the torque loss due to friction at 0 rpm. K_{TP} is called the friction torque vs pressure drop coefficient and it is defined as the gradient of the friction torque vs pressure curve of the hydraulic motor. $\omega_{threshold}$ is the threshold angular velocity for the motor-pump transition. It is a set value of a fraction of the nominal angular velocity. The tanh function is there to determine the direction of the shaft rotation. K_{TP} can be determined with the mechanical efficiency of the motor. The mechanical efficiency is η_m. Therefore, K_{TP} can be specified as:

$$K_{TP} = \frac{\Delta T_c * (1-\eta_m)}{\left(\frac{\Delta P_c}{q}\right)} \tag{20}$$

where ΔT_c is the torque difference from the torque vs power curve of the technical data sheet of the hydraulic motor, ΔP_c is the power difference for the torque difference.

Finally, an angular velocity source is used to control the angular velocity of the motor. With this source, the angular velocity of the motor can be specified through a physical signal input to the angular velocity source. To determine the angular velocity required, the ideal angular velocity must be computed and multiplied by the volumetric efficiency. Controlling the angular velocity is important because the

hydraulic motor should not exceed its maximum angular velocity and preferably stay well under the maximum angular velocity.

To model the start-up time, a Harrison curve is utilized. The Harrison curve is an s-shaped curve that can be utilized to approximate the start-up behaviour of a hydraulic motor (Michael, et al., 2012). Its form is presented in the next equation and the output is the actual angular velocity of the output shaft of the motor:

$$\omega = \frac{\omega_f}{2}\left(1 - \cos\left(\frac{t\pi}{t_s}\right)\right) for\ t \leq t_s \quad (21)$$

where ω_f is the steady-state angular velocity of the output shaft of the hydraulic motor and t_s is the start-up time of the hydraulic motor. Once steady state is reached, the angular velocity is:

$$\omega = \omega_f\ for\ t > t_s \quad (22)$$

$$\omega_f = \omega_{ideal}\eta_v \quad (23)$$

Finally, the mechanical power output is computed as follows:

$$P_M = T\omega \quad (24)$$

12.5. Power loss and Efficiency

Presented next are the formulas for the losses and the efficiency of the simulation.

The power loss in the hydraulic tube is determined by:

$$P_{LT} = \Delta pq \quad (25)$$

where P_{LT} is the power loss in the hydraulic tube.

The power loss in the hydraulic motor is computed as:

$$P_{LM} = P_H - P_{LT} - P_M \quad (26)$$

where P_{LM} is the power loss in the hydraulic motor, P_H is the hydraulic power input and P_M is the mechanical power output.

The total power loss, $P_{L,total}$, in the hydraulic system can be expressed as:

$$P_{L,total} = P_{LT} + P_{LM} \quad (27)$$

Any efficiency can be computed by dividing the energy output by the energy input. This concept can be applied to the hydraulic motor.

$$\eta_{s,m} = \frac{P_M}{(P_H - P_{LT})} \quad (28)$$

Where $\eta_{s,m}$ is the hydraulic motor efficiency.

The efficiency of the hydraulic system is represented in the following formula:

$$\eta_{s,total} = \frac{P_M}{P_H} \tag{29}$$

where $\eta_{s,total}$ is the total efficiency of the tube and the hydraulic motor combined.

With the MATLAB files presented in the Appendices B until F, the power loss and the efficiency of the simulations can be computed.

12.6. Reference blocks, clocks and solver configuration

Finally, a hydraulic reference block was added to the circuit for a practical reason: for the generation of a stable output of the motor. This reference ensures a stable outlet of the hydraulic motor such that the pressure difference is as desired. Furthermore, a mechanical rotational reference block was added since the angular velocity source utilizes the difference from the input to the output to the desired angular velocity. Therefore, with a mechanical rotational reference, the input is 0 and the output can be specified with the function described at the end of section 12.4.

Additionally, two clocks are included to accomplish time dependence in Simulink of the pressure input and the angular velocity. Lastly, a solver configuration is added as this is necessary for every simulation of a Simscape model.

12.7. Generator inclusion in the model

Finally, it was attempted to include the SCIG in the Simscape model. There is an 'Asynchronous Machine SI units' block in Simscape, which can be utilized to model the SCIG. However, due to limited time, this could not be realized within this research. Furthermore, there are several complexities in modelling generators. The complexities encountered are described for future research of the SCIG by Ocean Grazer.

Firstly, a gearbox must be included to convert the low angular velocity, high torque power supplied by the hydraulic motor to high angular velocity, low torque power that must be obtained by the generator. The optimal angular velocity is to be determined.

Next, there were complexities in the start-up behaviour of the generator. Since induction generators act a motor below their synchronous angular velocity, it was not determined how the generator would behave and how it should be connected in the model for angular velocities below the synchronous angular velocity.

Furthermore, the SCIG must first be excited to generate electricity. This could be done with a voltage source in Simscape; however, it is uncertain whether that is optimal as there are more options. If the voltage source is used, it must be customized such that it excites the generator properly and that the generator also remains excited. The excitation process is continuous; however, the exact nature, the working of the excitation process, and its modelling were not determined within the time limit.

Additionally, in general, generators are three-phase. This entails that there are three coils in the generator that create the magnetic field required to generate electricity. This brings extra complexities in modelling compared to single-phase machines.

The SCIG in Simscape consists of an electrical and a mechanical subsystem. Especially the working of the electrical subsystem is considered complicated, as the electrical subsystem itself consists of 13 more subsystems which are utilized to define the conversion of mechanical energy to electricity.

In conclusion, due to the limited time, the generator could not be modelled. Therefore, the factors that are to be considered were outlined to provide a starting point for further research in this area.

13. Validation

The model can be validated by face validity (Sargent, 2013). This entails that an individual with sufficient knowledge of the system reviews the model. The problem owner was approached to review the model. After inclusion of a sensitivity analysis, it was discussed that the model appears reasonable.

Furthermore, the validity of the model can be assessed by performing analytical calculations. Because the flow was critical for a tube diameter of 0.38 m, the hydraulic tube model could not be validated for this diameter. This is because the linear interpolation to compute the friction factor could not be done by hand. Therefore, the diameter of 0.35 m was used for the analytical calculations to validate the hydraulic tube model. The hydraulic tube model for turbulent flow was successfully validated as can be observed in Appendix G.

The hydraulic motor leakage and friction torque were also successfully validated in Appendix H. However, the ideal torque and therefore also the output torque could not be determined manually. This is because the manual calculation gives the ideal torque per revolution rather than the instantaneous torque that is shown in the simulation in Simscape. It is suspected that Simscape computes the instantaneous torque produced rather than the torque per revolution or second. Simscape possibly does this by calculating the instantaneous volumetric displacement at a very small section of time, which could not be derived manually. In conclusion, the energy losses in the hydraulic motor were successfully validated, however, the generated torque was not.

Lastly, the model was validated by parameter variability (Sargent, 2013). Parameters were adjusted in chapter 15, to observe the changes in the outputs. The changes in the outputs were as could be expected. The change in diameter of the tube significantly increased the pressure loss and the changes in efficiencies showed the decrease in the hydraulic motor.

14. Simulation

To simulate the model, several parameters must be specified. These were determined by utilizing data from the technical data sheet of the hydraulic motor and literature on high-pressure hydraulic tubes. However, first, the power inputs must be specified.

Since the real power inputs are unknown, the power inputs were determined from a similar high-pressure hydraulic system and discussion with the problem owner. Therefore, it is assumed that the fluid power delivered by the power take-off device is between 500 kW and 2000 kW.

From the technical data sheet of the CBM 3000 2200 8 port, the volumetric displacement was determined. The volumetric displacement of the CBM 3000 2200 8 port a set value of 0.138686 m^3/rev (Bosch Rexroth, 2019) (Bosch Rexroth, 2012). The maximum angular velocity of the CBM 3000 2200 8 port is 29 rpm (Bosch Rexroth, 2019). Therefore, the maximum flow rate through the hydraulic motor can be determined, such that this value will never be exceeded. The maximum flow rate through the motor is:

$$q_{max} = \frac{0.138686 * 29}{60} = 0.067 \text{ m}^3/\text{s}$$

Because it is not recommended by the manufacturer to run the motor at maximum capacity, a reduced flow rate obtained from literature was utilized. This flow rate is 60.0×10^{-3} m^3/s (Laguna, et al., 2014). With a sine wave, a varying input pressure range from 8.33 MPa to 33.3 MPa over 70 seconds was generated, to ensure losses for all power inputs from approximately 500 kW to 2000 kW are specified. The sine wave is designed such that the lower bound is exactly at 2.5 seconds because this is the start-up time determined for the hydraulic motor (Dasguptaa, et al., 2012). The pressure input is shown in figure 14.

$$p_{in} = 20.815 \times 10^6 + 12.485 \times 10^6 \sin\left(\frac{-0.062831853\pi(t + 13.41549)}{2}\right)$$

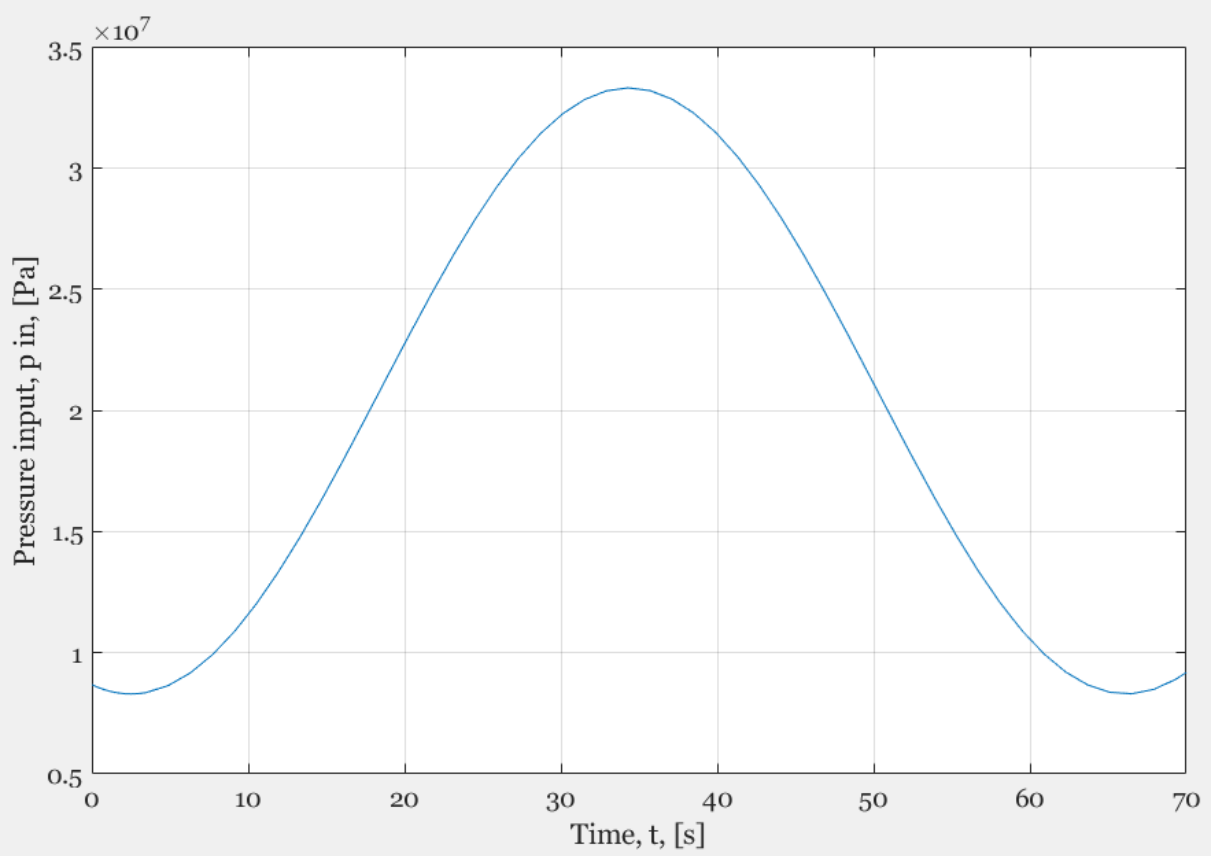

Figure 14: Fluctuating pressure input from the pressure source over time.

Firstly, parameters for the hydraulic fluid, such as the temperature and relative amount of trapped air must be specified. The relative amount of trapped air is the ratio of gas volume to the fluid volume. The relative amount of trapped air in the fluid is set to 0, this implies an ideal fluid. This is because at this point, the amount of trapped air could not be determined from data and the actual value should be close to 0 for hydraulic fluids. The temperature was set to 12 degrees Celsius as this is the mean water temperature in the North Sea (Gemiddelden, sd). In table 3, the parameters specified for the simulations of the hydraulic fluid block are displayed.

Parameter	**Value**	**Unit**	**Explanation**
Hydraulic fluid	Fluid MIL-F-83282	-	Fluid type
The relative amount of trapped air	0	-	Specified as the ratio of gas volume at normal conditions to the fluid volume in the tube. For ideal fluid 0.
System temperature	12	Degrees Celsius	Mean water temperature of the North Sea

Viscosity derating factor	1	-	This can be used to adjust the viscosity of the fluid if necessary. Between 0.5 and 1.5. 1 if no adjustment is needed.
Pressure below absolute zero	-	-	Not relevant since absolute zero will not be reached.

Table 3: Parameters and inputs required for the hydraulic fluid.

For the computations of the pressure loss, the hydraulic resistive tube in Simscape requires several inputs for the parameters. A range of flexible tube diameters and pressures they can resist was obtained by Guo (Guo, et al., 2013). The range specified is of hydraulic offshore flexible tubes with a diameter of 0.06350 m to 0.4064 m. With maximum pressures of up to 103.4 MPa to 27.58 MPa for the given diameters respectively. Since the relation between the tube diameter and the pressure is uncertain in this specified range and the maximum diameter is unusable since it does not function for the pressure, losses for several diameters are determined. However, for this simulation, a linear relationship between the diameter of the tube and the pressure is assumed. Therefore, a diameter of 0.38 m is picked since this is the pressure maximum diameter of the tube if the relationship between the diameter of the tube and the pressure is linear. The gradient of this graph is specified as:

$$\frac{\Delta D}{\Delta p_{allowed}} = \frac{(0.4064-0.06350)}{(27.58\times10^{6}-103.4\times10^{6})} = -4.522 \times 10^{-3}\ \text{m/Pa}$$

Where ΔD is the change in diameters and $\Delta p_{allowed}$ the change in the maximum allowed pressure. Therefore, for a maximum pressure of 33.3 MPa, the maximum diameter is then:

$$D_H = 0.4064 + (33.3 - 27.58) * (-4.522e^{-3}) = 0.38\ \text{m}$$

The hydraulic flexible tubes consist of multiple layers for reinforcement and have an inner layer of rubber. Therefore, the roughness of rubber is also utilized as an input. An overview of the parameter inputs is specified in Table 4.

Parameter	**Value**	**Units**	**Explanation**
Tube cross-section type	Circular	-	Circular tubes will be used
Tube internal diameter	0.38	m	-
Geometrical shape factor	64	-	Shape factor regarding the type of tube. 64 for circular tubes.
Tube length	70	m	-
The aggregate equivalent length of local resistances	0	m	Additional length due to obstacles such as bends and valves. These are not present in this system.
Internal surface roughness height	6×10^{6}	m	Internal roughness of the tubes for flexible smooth rubber (Neutrium, 2012)

Laminar flow upper margin	2000-[-]	-	
Turbulent flow lower margin	4000	-	

Table 4: Parameters and input values of the hydraulic tube.

In figure 15, the pressure loss in the tube is depicted. It is time dependant because if there is no flow rate when the motor is not functioning yet, there can be no pressure loss. Furthermore, if observing closely, it can be noted that the pressure loss slightly increases for higher pressure inputs. However, this increase is very limited. Especially when realizing that the influence of approximately 880 Pa of pressure loss in the tube is already of minor influence compared to the total pressure input of 8.33 to 33.3 MPa. Furthermore, the power loss over the tube is depicted in figure 17, compared to the inputs of 500 to 2000 kW, the loss of approximately 53 W over the hydraulic tube is very minimal.

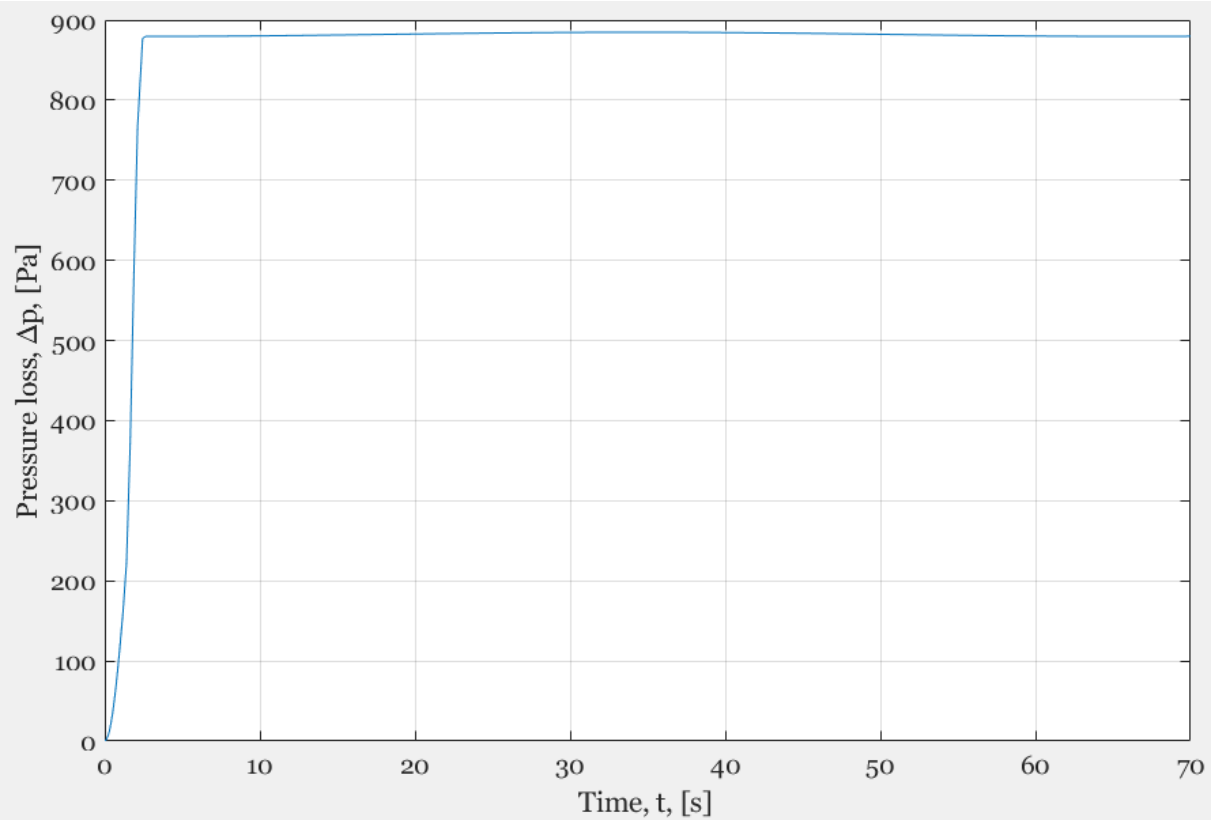

Figure 15: Pressure loss in the hydraulic tube over time.

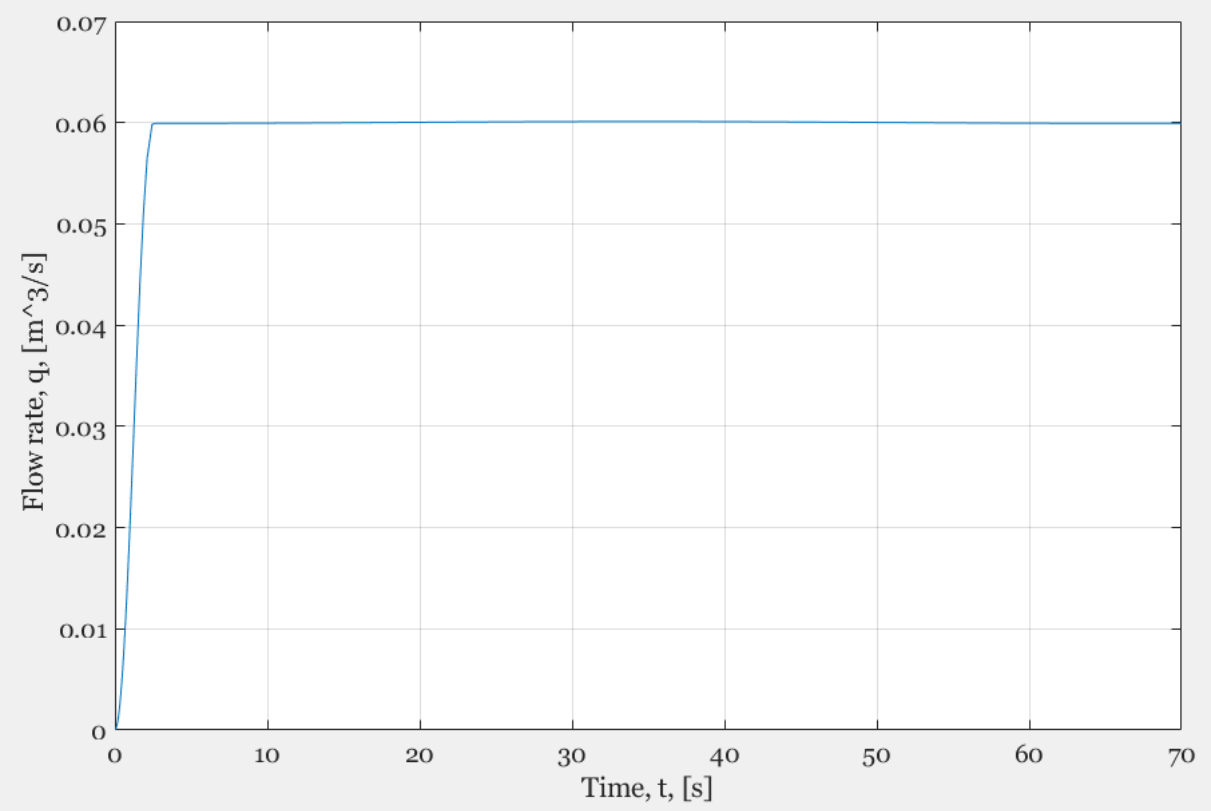

Figure 16: Flow rate in the hydraulic tube over time.

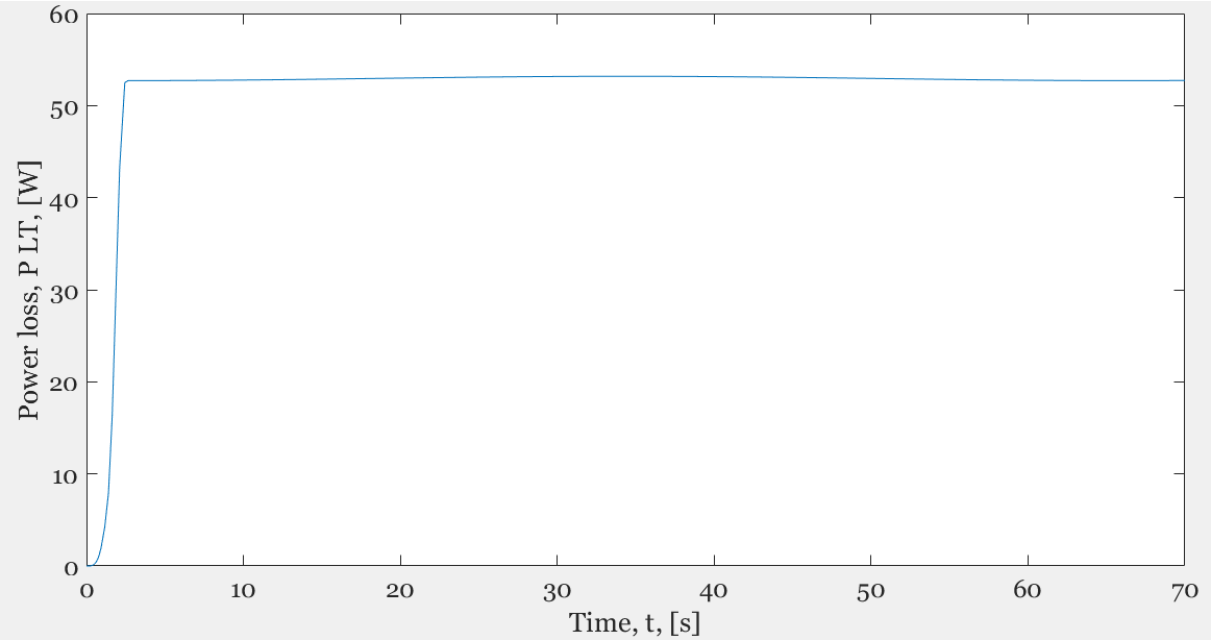

Figure 17: Power loss in the hydraulic tube over time.

Next, from the technical data sheet, the volumetric efficiency of the hydraulic motor, the nominal pressure loss and the nominal angular velocity were determined. The volumetric efficiency can be computed from the leakage in m^3 per minute. From the datasheet, the leakage is determined to be 15.0×10^{-3} m^3/min which is 0.250×10^{-3}

m^3/s. The steady-state flow rate is 60.0×10^{-3} m^3/s. Therefore, the volumetric efficiency is:

$$\eta_v = \frac{60.0\times10^{-3} - 0.250\times10^{-3}}{60.0\times10^{-3}} = 0.996$$

furthermore, the no-load torque is the torque produced while no angular velocity is produced. It was not found in the technical datasheet. However, it was estimated through communication with Bosch Rexroth that the general starting torque loss is 20%. Since the starting torque is unknown, the no-load torque was derived from the minimum torque generated. The torque for a no-load torque of 0 was determined, to derive the no-load torque from the ideal torque with the percentage obtained from Bosch Rexroth. The minimal torque, so the torque at the lowest pressure input is 180×10^3 Nm.

$$T_0 = 0.20 * 180 \times 10^3 = 36 \times 10^3 \text{ Nm}$$

Additionally, K_{TP} is determined. Its value is approximated because it was determined from the friction vs power curve and therefore the power had to be divided by the flow rate to obtain a value for the pressure. Since the flow rate is a function of Δp_m, it is not a fixed value. Therefore, it is determined for both 700 kNm and 1.904MW and at 370 kNm and 1.007 MW respectively. Furthermore, mechanical efficiency is 98% for steady-state power inputs. For both inputs, a value of 0.00044 was obtained as demonstrated below. Therefore, this gradient is utilized in the simulation.

$$K_{TP} = \frac{700\times10^3\times(1-0.98)}{\left(\frac{1.904\times10^6}{60.0\times10^{-3}}\right)} = 0.00044 \qquad K_{TP} = \frac{370\times10^3\times(1-0.98)}{\left(\frac{1.007\times10^6}{60.0\times10^{-3}}\right)} = 0.00044$$

Since no data on the relation between the volumetric efficiency and the nominal values of the viscosity and the density could be determined, the nominal values are set equal to the actual density and viscosity of Fluid MIL-F-83282. Because of the dependence of the Hagen Poiseuille coefficient on the ratio between the nominal and actual density and viscosity, the temperature of the fluid being unextreme and the small change in density and viscosity due to fluctuations of the temperature, the ratio is expected to stay close to 1.

In the following table the required inputs of the fixed displacement motor are presented:

Parameter	Value	Unit	Explanation
Displacement	0.138686	m^3/rev	The fixed volumetric displacement of the motor per revolution.
Leakage and friction parameterization	Analytical	-	This option is set for the analytical calculations of the losses in the motor.
Nominal shaft angular velocity	26	Rpm	The angular velocity of the shaft in the simulations.
Nominal pressure loss	33	MPa	The pressure loss from the inlet to the outlet of the motor.
Nominal kinematic viscosity	51.2014	cST	The kinematic viscosity of the selected hydraulic fluid at 12 degrees C.
Nominal fluid density	842.96	Kg/m^3	The fluid density of the hydraulic fluid at 12 degrees C.
Volumetric efficiency at nominal conditions	0.996	-	The volumetric efficiency of the CBM 2000 1200 at 35 MPa, determined from the technical datasheet.
No-load torque	36×10^3	Nm	The torque required to overcome friction and initiate rotation for the CBM 3000 2200.
Specific torque	0.00044	Nm/Pa	
Check if lower side pressure violating minimum valid condition:	None/warning	-	Check whether the outlet pressure does not reach a value below 0.

Table 4: Parameters and inputs required for the fixed displacement motor.

To control the angular velocity of the hydraulic motor the angular velocity must be specified through the angular velocity source. The ideal angular velocity to achieve the desired flow rate is specified as:

$$\omega_{ideal} = \frac{60.0\times10^{-3}}{0.138686} * 60 = 26.0 \text{ rpm}$$

the steady-state angular velocity is, therefore, determined to be:

$$\omega_f = 26.0 * 0.996 = 25.9 \text{ rpm } \textit{for } t>2.5$$

and the angular velocity while starting is therefore defined with the following function.

$$\omega = \frac{25.9}{2}\left(1 - \cos\left(\frac{t\pi}{2.5}\right)\right) \text{ rpm } \textit{for } t\leq2.5$$

In figure 18, the torque loss due to friction is displayed. The loss depends on the pressure and therefore the peak in the loss of friction is at the time of maximum

pressure. Furthermore, there is already a torque loss when the rotation of the output shaft is initiated because there already is friction present before rotating commenced. Because of the dependence of the friction torque on pressure, more losses were expected for higher pressures.

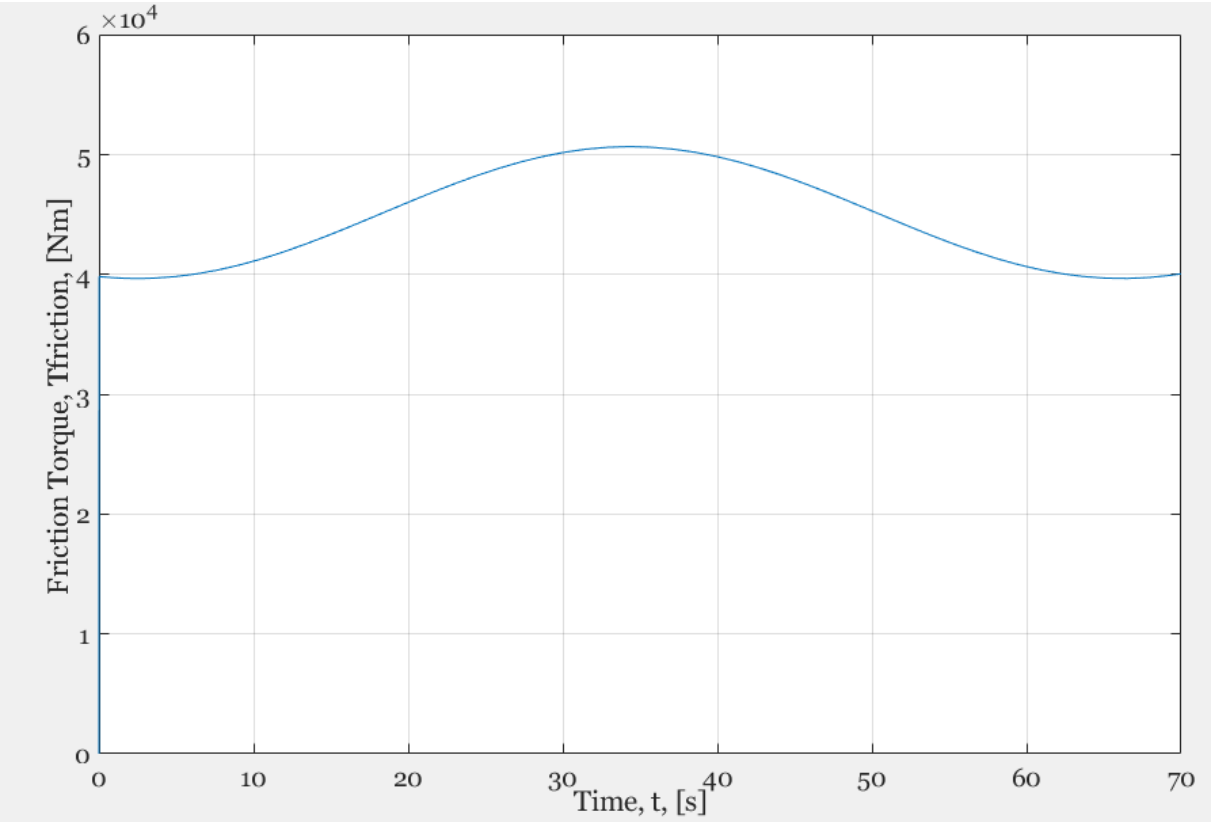

Figure 18: Torque loss due to friction in the hydraulic motor over time.

Next, the leakage from the motor is displayed in Figure 19. Leakage flow is instantly visible because the leakage flow rate is a function of the pressure difference over the hydraulic motor and not of the flow rate through the hydraulic motor. It is visible that the leakage increases significantly for higher pressures. However, it remains relatively low compared to the flow rate through the motor due to the high volumetric efficiency.

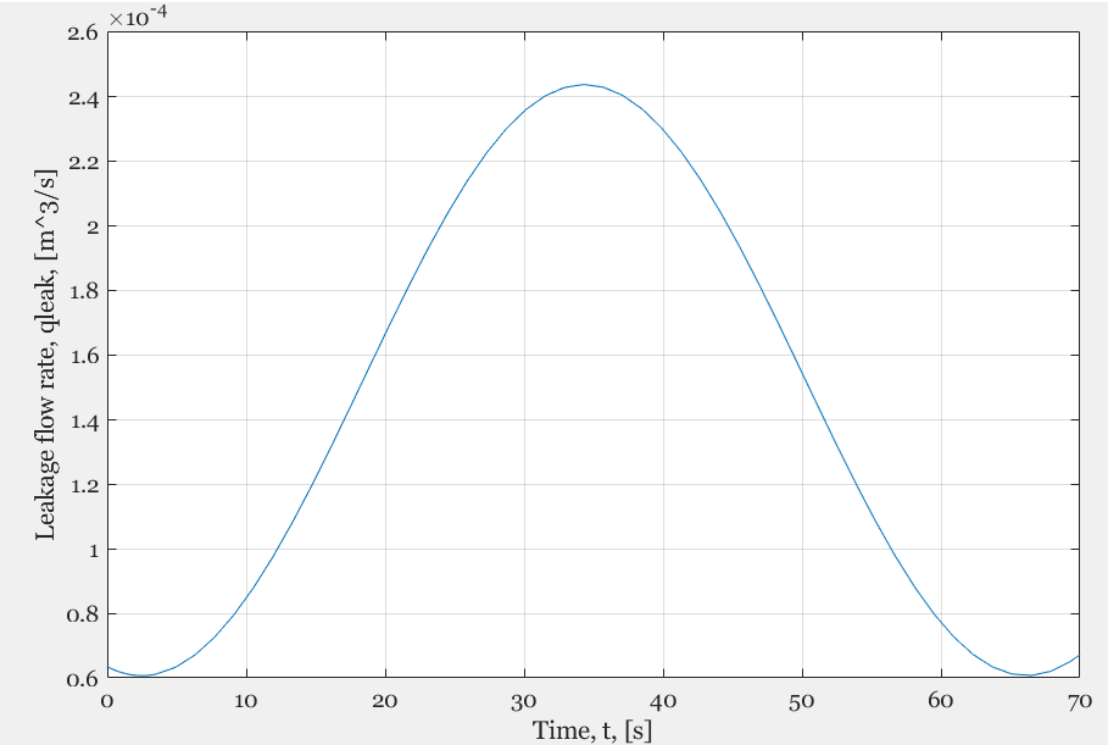

Figure 19: Leakage flow rate from the motor over time.

In figure 20, the angular velocity of the output shaft is displayed. It is depicted that the hydraulic motor takes 2.5 s to reach the desired steady-state angular velocity.

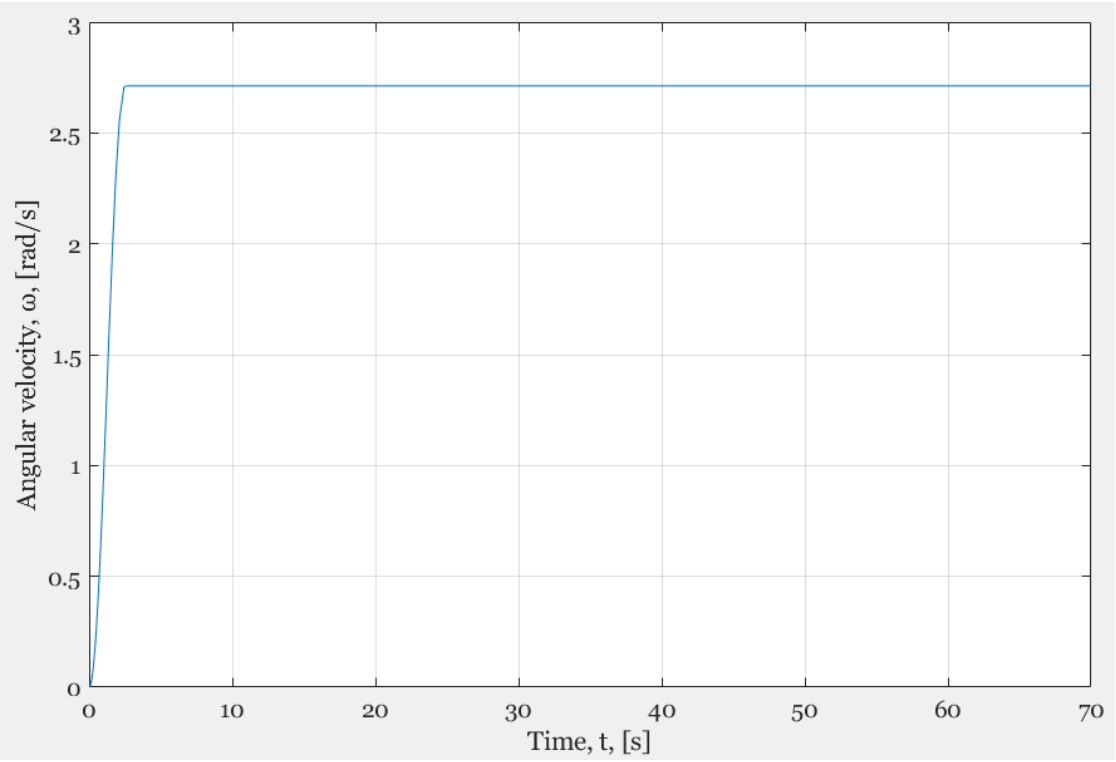

Figure 20: Controlled angular velocity of the output shaft of the hydraulic motor over time.

In figure 21, the hydraulic power input and the mechanical power output of the hydraulic motor are depicted. It can be observed that the difference in the hydraulic motor loss does not change significantly as the leakage and friction torque fluctuations are relatively minor compared to the total mechanical power output. However, in figure 22, the difference between the mechanical power output and the hydraulic power output is demonstrated and it is depicted that the losses in the motor fluctuate with approximately 37 kW. The fluctuations in the losses are relatively small compared to the fluctuations in the total power inputs and outputs. This is mainly due to the high efficiencies obtained from the technical data sheet of the hydraulic motor provided by the manufacturer. Lastly, in figure 23 the efficiency of the hydraulic motor is illustrated in a graph. Because the fluctuations in the power losses are relatively small and the fluctuations in the power inputs large, the efficiency increases for increases in power.

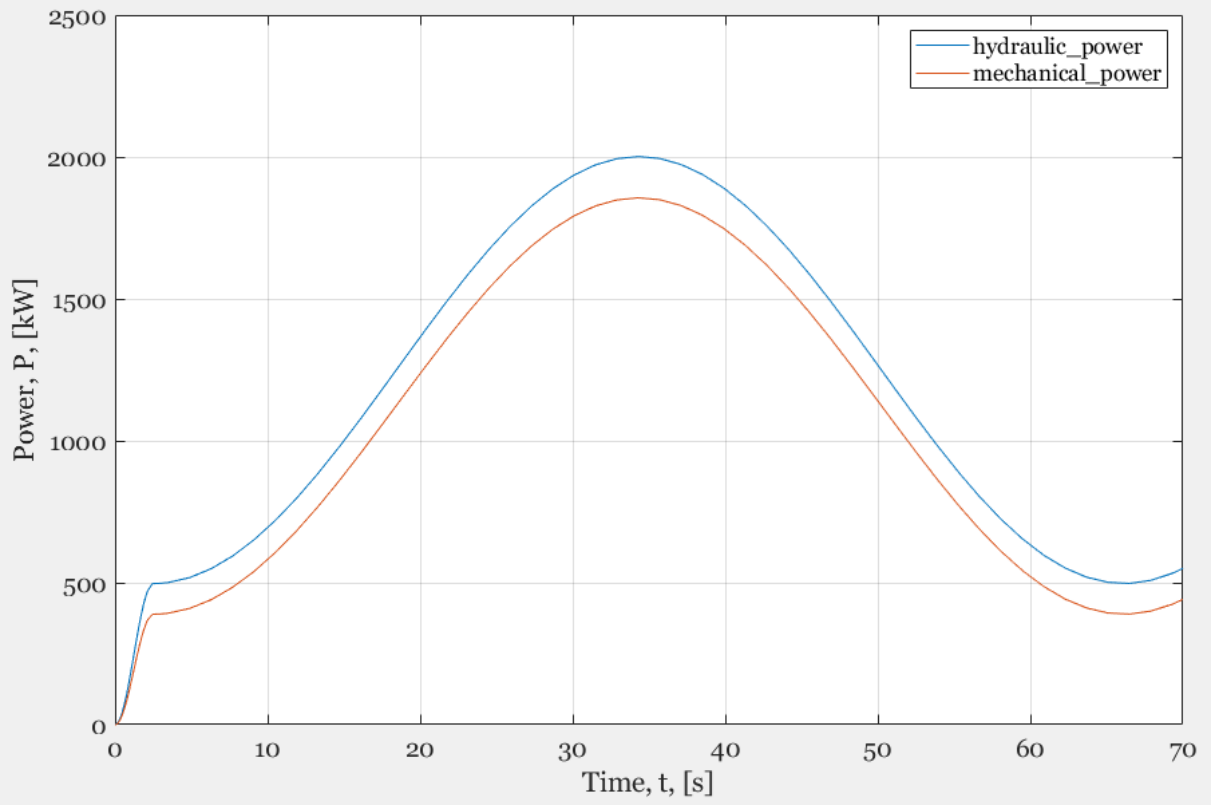

Figure 21: Hydraulic power input and mechanical power output of the hydraulic motor over time.

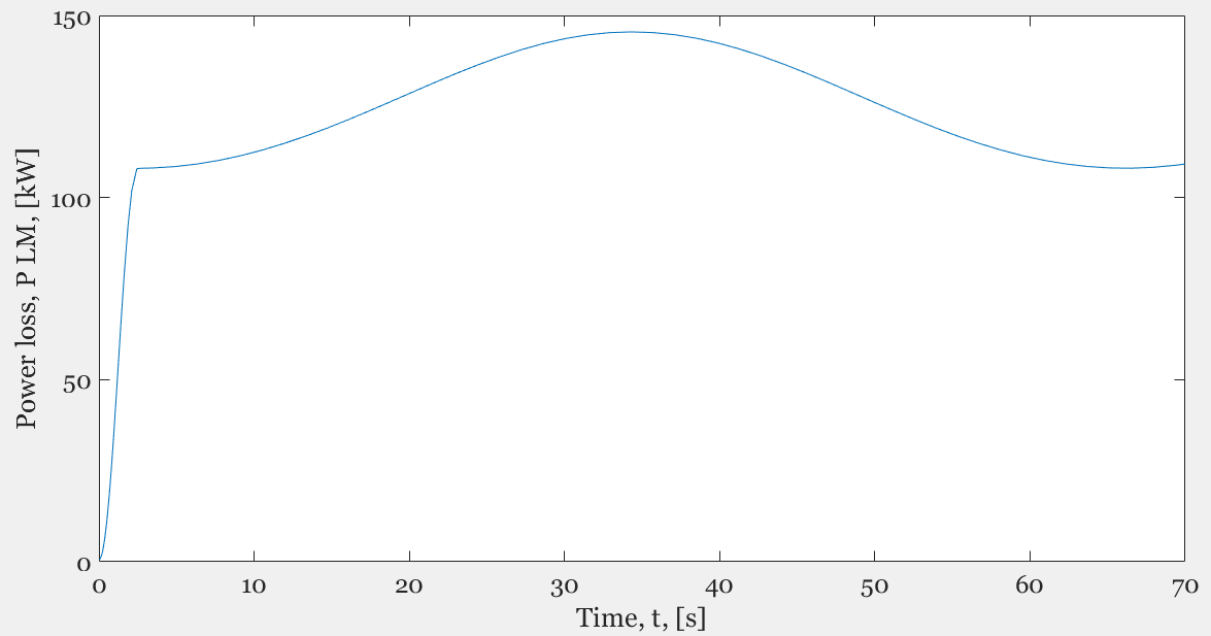

Figure 22: Difference between the hydraulic power input and the mechanical power output over time.

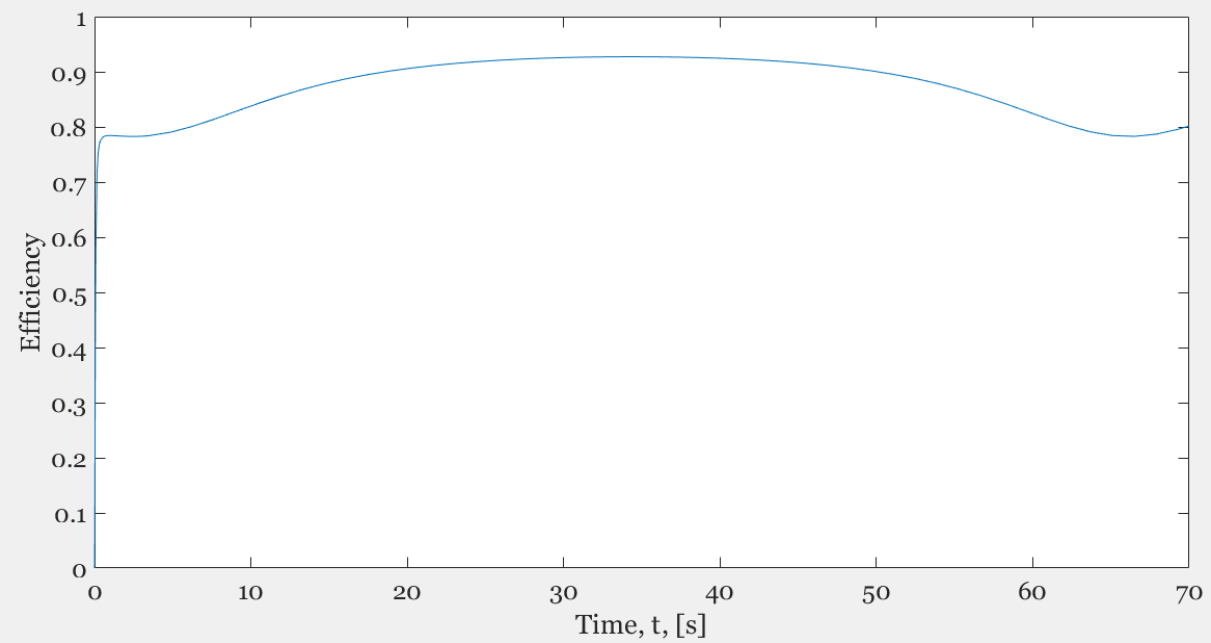

Figure 23: Efficiency curve of the hydraulic motor over time.

Finally, the total power loss is depicted in figure 24. Furthermore, the efficiency of the model is presented in figure 25. Naturally, because the power loss in the hydraulic tube is relatively low, the efficiency curve is almost identical to the efficiency curve of the hydraulic motor.

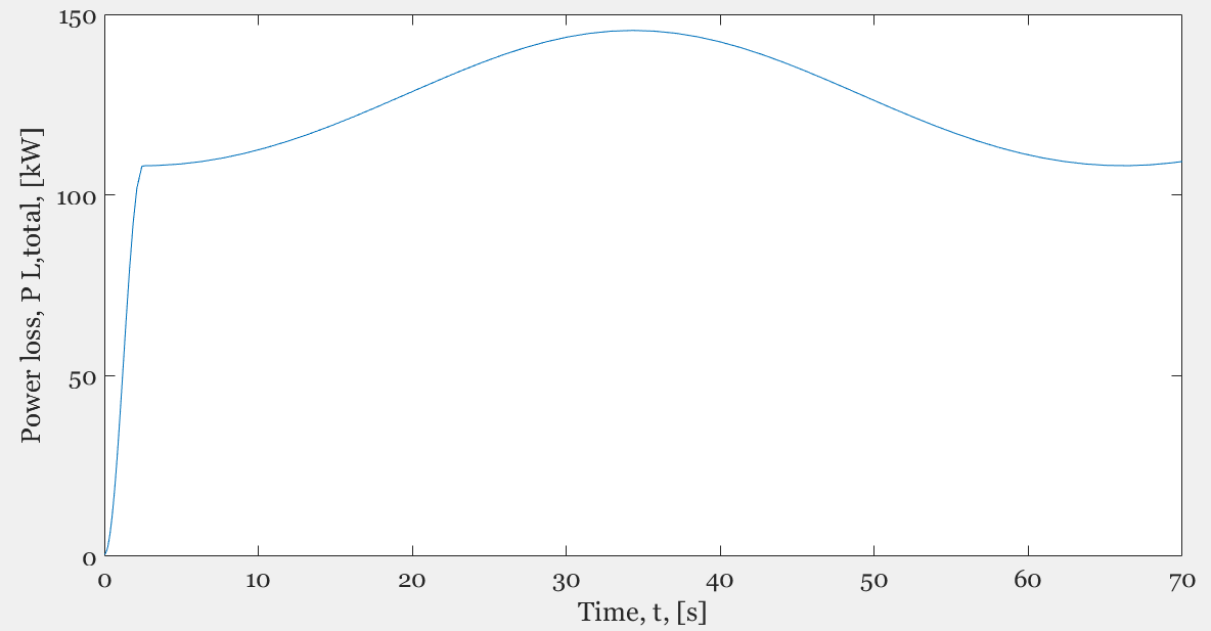

Figure 24: Power loss of the hydraulic motor and the hydraulic tube over time.

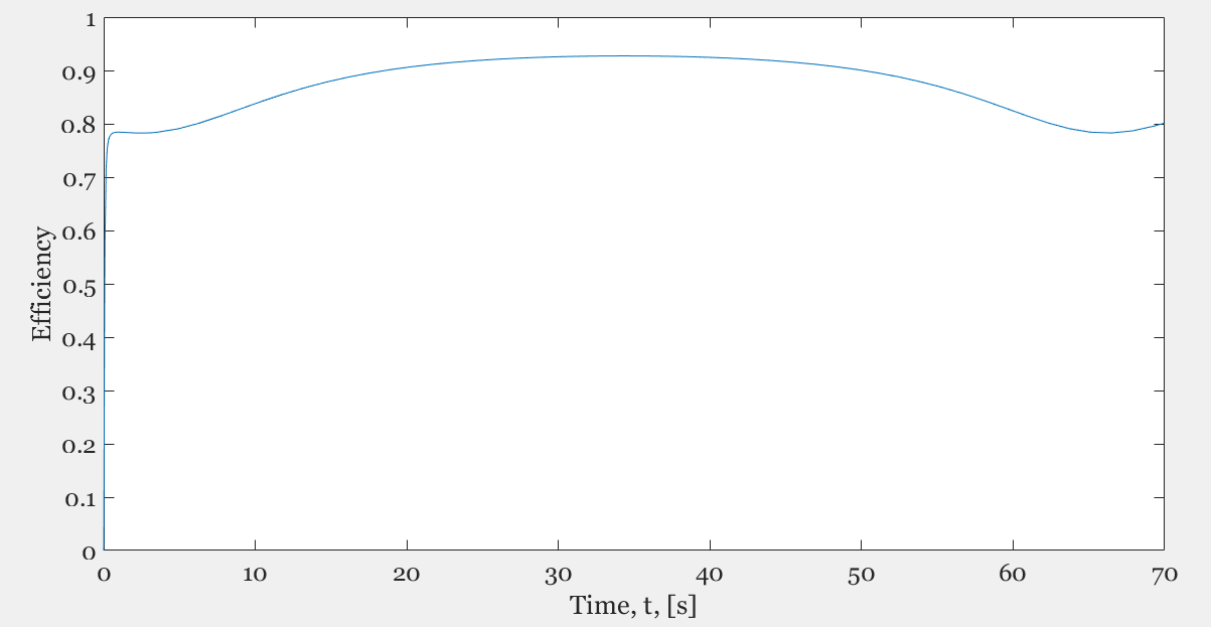

Figure 25: Efficiency curve of the hydraulic motor and the hydraulic tube over time.

15. Sensitivity analysis

To observe the influences of changes in the parameters of the model, a sensitivity analysis is performed. Parameters are changed and the differences in energy loss and efficiency are depicted.

15.1. Hydraulic tube diameter impact

The pressure loss in the hydraulic tube depends strongly on the diameter of the tube. The larger the diameter of the tube, the smaller the pressure loss in the tube. It has been concluded that a diameter of 0.4064 meters was a maximum of hydraulic tubes manufactured for offshore flexible tubes (Guo, et al., 2013), however, this is not feasible with the maximum pressure utilized in this research. Therefore, previously a linear relationship between the diameter of the tube and the maximum allowed pressure was assumed. However, this might not be the case. Therefore, two other diameters are investigated. Losses are expected to increase as the diameter of the tube becomes narrower. Diameters of 0.35 m, 0.30 m and 0.25 m are tested, and the pressure loss is shown in Figures 26, 27 and 28 respectively.

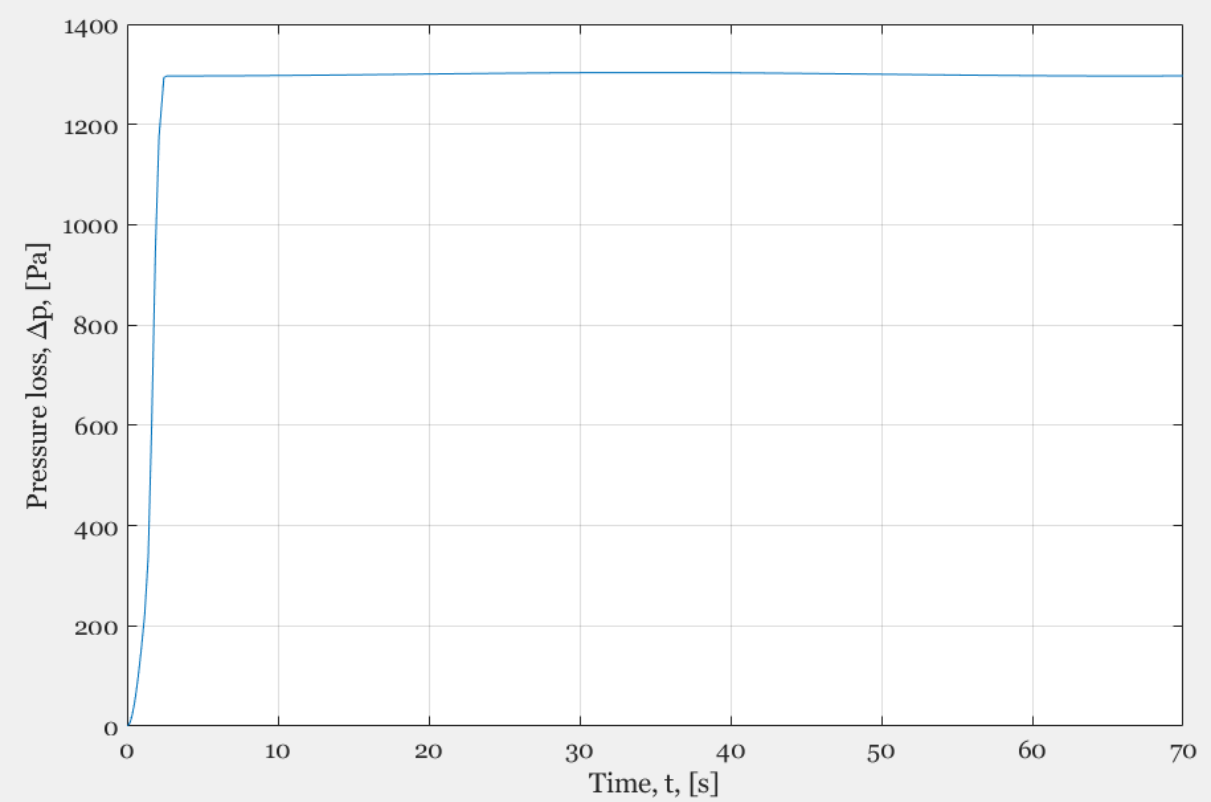

Figure 26: Pressure loss for a tube diameter of 0.35 m.

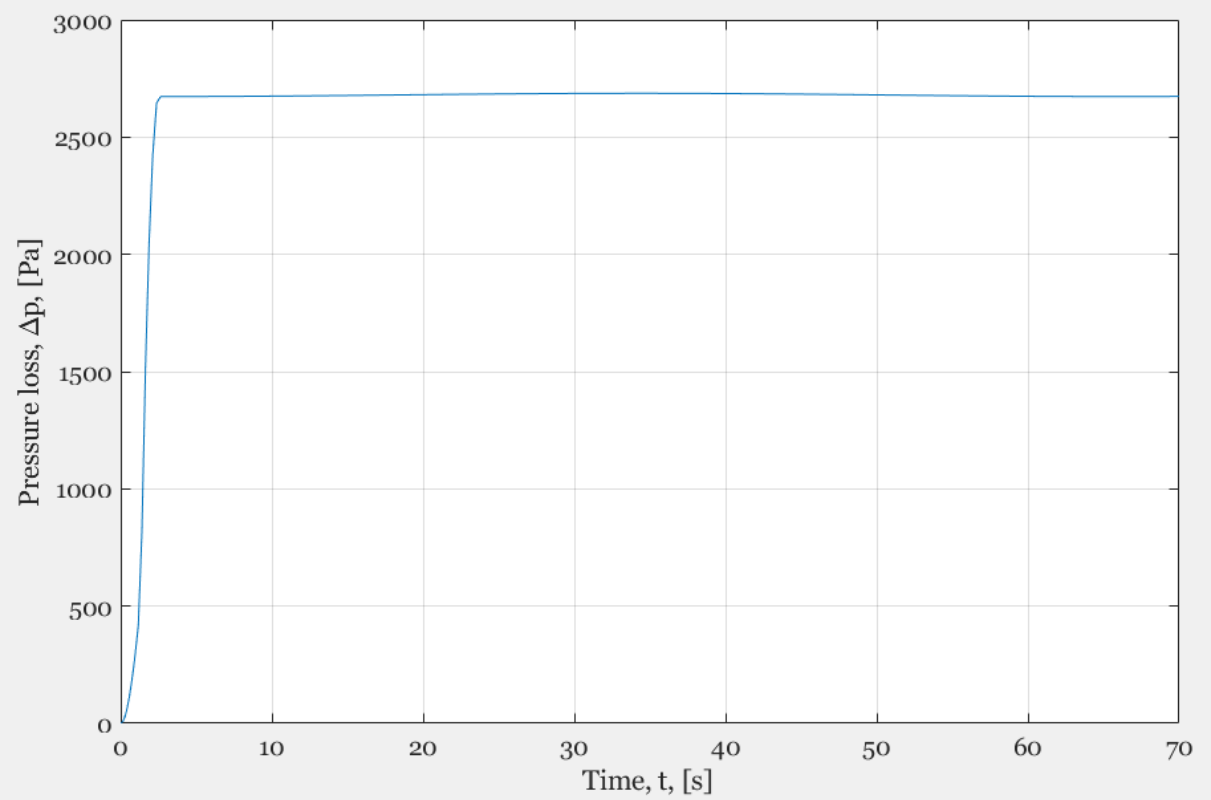

Figure 27: Pressure loss for a tube diameter of 0.30 m

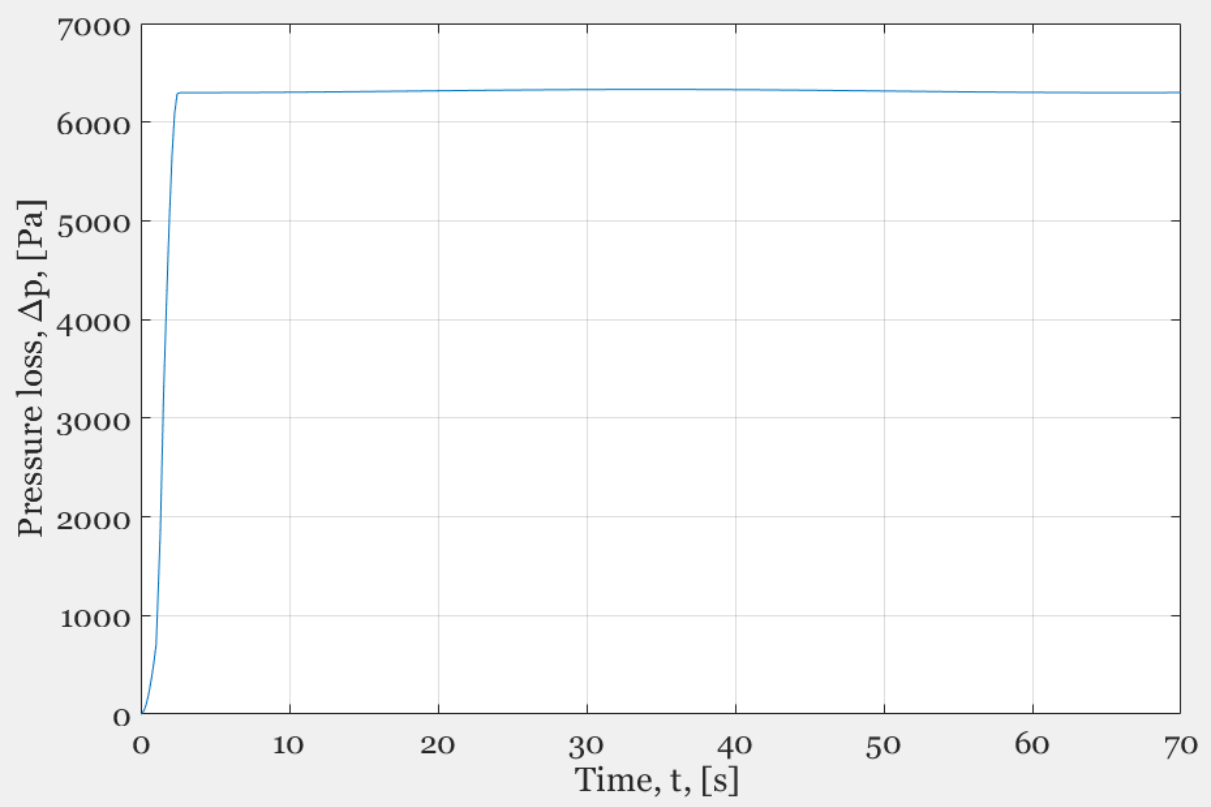

Figure 28: Pressure loss for a tube diameter of 0.25 m

It can be concluded that the pressure loss in the hydraulic tube rapidly increases as the diameter of the tube becomes narrower. This is related to the velocity of the fluid that is increased for the smaller diameter. When the velocity increases, Reynold's number increases and therefore flow becomes turbulent. Therefore, to minimize losses, Ocean Grazer needs to use the widest diameter possible.

15.2. Hydraulic motor volumetric and mechanical efficiency impact

The efficiencies utilized for the simulation presented in chapter 14 were determined from data of the hydraulic motor manufacturer. Because the values may be higher than data derived from testing, the effect of adjusting these values is examined. The hydraulic tube diameter was adjusted back to 0.38m.

The volumetric efficiency can be adjusted in the hydraulic motor block in Simscape. Furthermore, the angular velocity of the hydraulic motor must be adjusted such the maximum flow rate is not reached. Preferably the angular velocity ensures that the flow rate stays well under the maximum flow rate. When the volumetric efficiency is adjusted to the default value in Simscape of 0.92, the steady-state angular velocity is adjusted too.

$$\omega_f = 26.0 * 0.92 = 23.9 \text{ rpm } \textit{for } t>2.5$$

$$\omega = \frac{23.9}{2}\left(1 - \cos\left(\frac{t\pi}{2.5}\right)\right) \text{ rpm } \textit{for } t \leq 2.5$$

The influence of the lower volumetric efficiency on hydraulic motor efficiency can be observed in Figure 29. The increase in power loss due to an increased leakage especially influences the efficiency at the point of maximum power input. The maximum power input is no longer the most efficient point. There is a point of maximum efficiency at approximately 22 s and 45 s. This is when the hydraulic power input is approximately 1500 kW. Therefore, it is concluded that the point of maximum efficiency shifts when the volumetric efficiency drops significantly. At the point of maximum efficiency, an increase in pressure difference over the motor does not increase efficiency anymore. Whereas in the simulation presented in chapter 14, the point of maximum efficiency was at the point of maximum power input.

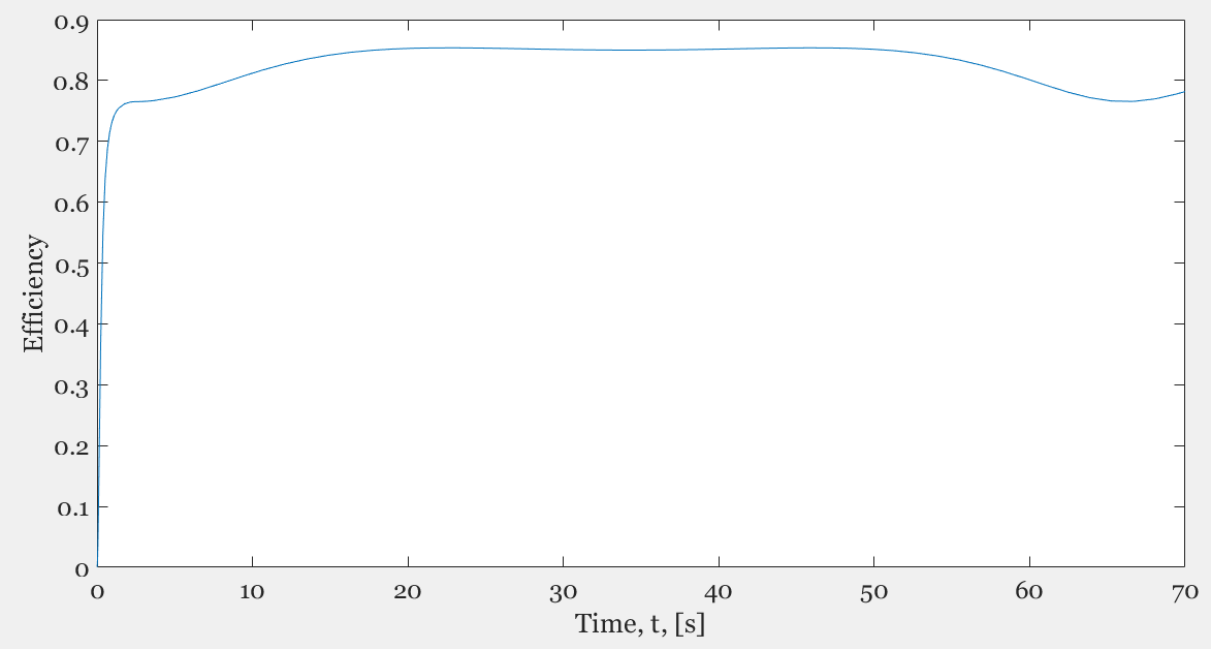

Figure 29: Efficiency curve of the hydraulic motor for a volumetric efficiency of 0.92.

Next, the influence of mechanical efficiency is examined. For this, the mechanical efficiency was adjusted to 0.92 and the volumetric efficiency was adjusted back to 0.996. When the mechanical efficiency is increased, the value of K_{TP} will increase. This entails that the torque lost due to friction increases.

$$K_{TP} = \frac{700\times10^3*(1-0.92)}{\left(\frac{1.904\times10^6}{60.0\times10^{-3}}\right)} = 0.0018 \qquad K_{TP} = \frac{370\times10^3*(1-0.92)}{\left(\frac{1.007\times10^6}{60.0\times10^{-3}}\right)} = 0.0018$$

The results are displayed in figure 30. This time, the point of maximum efficiency is still at the point of maximum power input. The efficiency curve is shifted downwards for the adjusted mechanical efficiency. This is due to the increase in power loss due to friction.

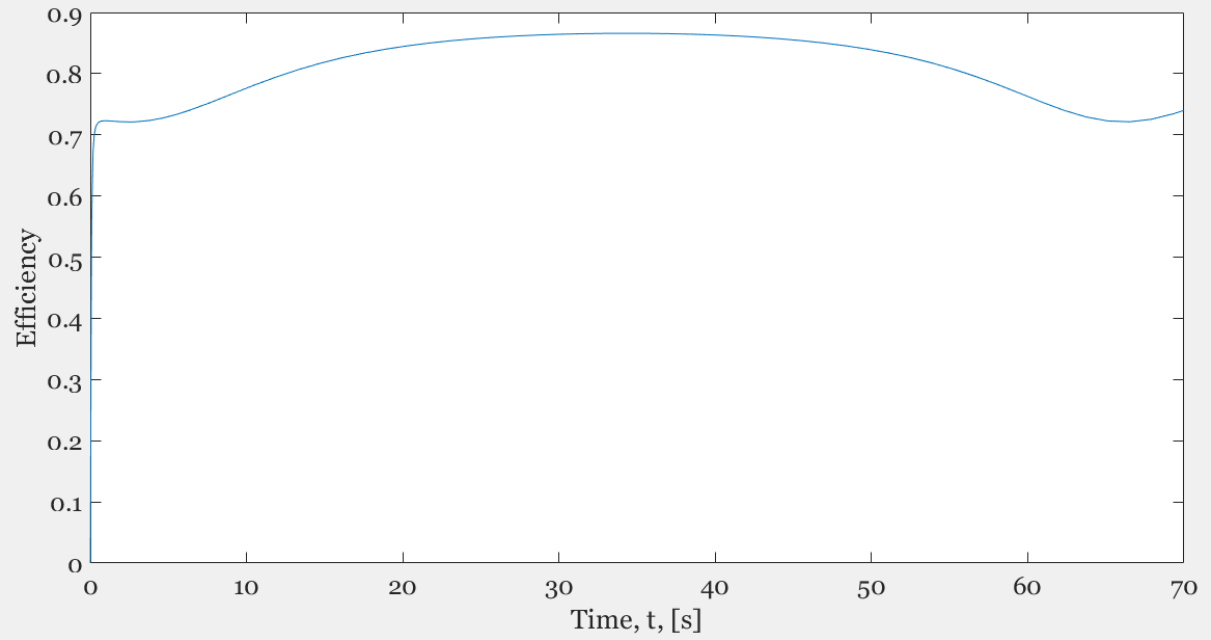

Figure 30: Efficiency of the hydraulic motor for a mechanical efficiency of 0.92.

16. Discussion

Individual components required for the system Ocean Grazer has in mind were evaluated. From technical requirements, it was determined that a radial piston motor is to be utilized as a hydraulic motor. This hydraulic motor was modelled dynamically using Simscape. The power in and outputs were obtained and the losses due to friction and leakage were presented for different pressure inputs. Furthermore, the pressure loss in the hydraulic tube was determined. It can be observed that the losses in the hydraulic tube are relatively small compared to the losses in the hydraulic motor. Additionally, it was determined that the radius must be as large as possible to minimize the energy loss in the hydraulic tube. When Ocean Grazer is considering implementation of the hydraulic system, manufacturers can be contacted to discuss the widest radius allowed for the maximum pressure. This could then simply be modified in the model to obtain the losses for such a radius. Lastly, the HFD synthetic ester MIL-F-83282 is utilized as a hydraulic fluid. This is because the use of an HFD synthetic ester suits the hydraulic motor. In conclusion, the type of hydraulic motor, its efficiency, the radius of the tube, the hydraulic fluid and the power losses in the system combined were successfully determined from literature and through simulations of the model.

Additionally, PATs and types of generators, that could be implemented in the Ocean Battery, were evaluated. Because no research had been performed by Ocean Grazer on PATs and generators yet, uncertainties regarding the use of either a PAT or a separate pump and turbine and the complexity that lies within selecting the machinery from literature, an outline of the characteristics was provided and the available types of generators were described rather than electing an optimal machine. The initial idea was to select the optimal machine and include it in the model, however, this was not attainable within the time frame. For the final selection of PATs or a separate pump and turbine, additional research should take place on the comparison of the two options. When that comparison has been developed, the optimal type of generator can be determined because the generator must interact with both the PAT or turbine and the hydraulic motor. Furthermore, to select the optimal generator, quantitative data must be obtained by for example testing. Little data is provided by both manufacturers and operators on the machines. Mainly because of the little data provided, it is strongly advised in literature sources concerning both PATs and generators to test the machines in similar circumstances to the circumstances they will be used in before implementing it in the Ocean Battery design. Furthermore, it is recommended to research the types of generators recommended and perform a quantitative analysis of their advantages and disadvantages and include the estimated frequency of maintenance on the Ocean Battery in this research.

Furthermore, in Appendix A the required connection to the electricity grid is discussed. This was not within the research scope however it was encountered and might be useful for Ocean Grazer in the future. Therefore, it is included in the Appendix.

Additionally, it must be noticed that the model presented in this research does not contain an entire hydraulic connection between the WEC and the Ocean Battery. This model must still be combined with a model of the harvested wave energy converted to fluid power to determine the efficiency of the total hydraulic system connecting the WEC and the Ocean Battery.

Finally, it is concluded that selecting the optimal machinery and modelling the system including a generator and PAT or separate pump and turbine was a task too extensive within the time frame and without testing facilities. The hydraulic motor and hydraulic tube have been modelled successfully. The pressure loss in the tube slightly increases as pressure increases. Furthermore, the torque and leakage loss in the motor also increases with the pressure, however efficiency increases as the pressure input increases. This is because, in the simulation, the loss that is dependent on the pressure is relatively small due to the high efficiencies obtained from the data of the motor manufacturer.

16.1. Limitations

In the simulation that is presented in chapter 14, the limitations consist of the efficiency data inputs are presumably biased and the power inputs are assumptions. The data obtained from the technical data sheet is delivered by the manufacturer, therefore the performance data is likely to be higher than data derived experimentally. Additionally, the exact power inputs are yet unknown and therefore assumed, however, this can be adjusted without complications.

Furthermore, in the model, the initiation of the angular movement of the hydraulic motor is an approximation of the actual initiation behaviour. Additionally, Simscape contains several limitations. The limitations consist of Simscape requiring several static input values whilst the system is dynamic. For example, mechanical and volumetric efficiency is specified statically. However, in practice, the efficiencies will vary for different loads instead of being constant. Additionally, it was not possible to tie the output pressure of the hydraulic motor to a minimum other than 0 and therefore the pressure difference required by the motor was utilized as an input. However, this limits the pressure loss in the hydraulic tube. Lastly, it is a limitation of Simscape that several computations are not visible for the user, such as the generated torque by the hydraulic motor and the pressure loss for critical flow in the hydraulic tube. Therefore, these parts could not be validated. Altogether, it appeared that Simscape did contain some advantages, however, it also included several disadvantages that were discovered while proceeding through the stages of developing the model.

17. Conclusion

In this paper, the efficiency of a hydraulic system containing a hydraulic tube and a hydraulic motor was determined. The efficiency of the considered hydraulic system ranged from 78% to 93%. Additionally, it was concluded that a radial piston motor is the only suitable hydraulic motor for the Ocean Grazer system and that the hydraulic tube diameter should be as high as possible, however, must certainly be less than 0.4064 m. It is concluded that the efficiency of the hydraulic system predominantly depends on the hydraulic motor. Furthermore, an evaluation of different applicable generator types is presented and the advantages and disadvantages of using PATs in the Ocean Battery are outlined. With the current knowledge about the Ocean Battery and qualitative reasoning, a Squirrel Cage Induction Generator is recommended for the Ocean Grazer system. Alternatively, a Doubly Fed Induction Generator could present a feasible option.

18. References

Alnasir, Z. & Kazerani, M., 2013. An analytical literature review of stand-alone wind energy conversion systems from generator viewpoint. *Renewable and Sustainable Energy Reviews,* Volume 28, pp. 597-615.

Barbarelli, S., Amelio, M. & Florio, G., 2017. Experimental activity at test rig validating correlations to select pumps running as turbines in microhydro plants. *Energy Conversion and Management,* Volume 149, pp. 781-797.

Baroudi, J. A., Dinavahi, V. & M.Knight, A., 2007. A review of power converter topologies for wind generators. *Renewable Energy,* 32(14), pp. 2369-2385.

Binama, M. et al., 2017. Investigation on pump as turbine (PAT) technical aspects for micro hydropower schemes: A state-of-the-art review. *Renewable and Sustainable Energy Reviews,* Volume 79, pp. 148-179.

Bosch Rexroth, 2012. *Radial piston hydraulic motor Type Hägglunds CBM*. [Online] Available at: https://products4engineers.nl/images/default/5RV4jc-pdf.pdf [Geopend April 2020].

Bosch Rexroth, 2019. *Bosch Rexroth Industrial Hydraulics Motors*. [Online] Available at: https://www.boschrexroth.com/en/xc/products/product-groups/industrial-hydraulics/motors [Geopend April 2020].

Bosch Rexroth, 2019. *Radial Piston Hydraulic motor Hägglunds CBm*. [Online] Available at: https://brmv2.kittelberger.net/borexmvz2-internet/pdfDownloadInternet.jsp?fn=RE15300_2019-08_POD.pdf&lvid=1214165&mvid=14627& [Geopend April 2020].

Budris, A. R., 2011. *Case History: Pumps as Turbines in the Water Industry,* sl: WaterWorld.

Carravetta, A., Houreh, S. D. & Ramos, H. M., 2018. *Pumps as Turbine*. sl:Springer International Publishing.

Chapple, P., 2015. *Principles of Hydraulic System Design*. Second Edition red. New York: Momentum Press.

Circuit Globe, 2018. *Induction Generator*. [Online] Available at: https://circuitglobe.com/induction-generator.html [Geopend May 2020].

Circuit Globe, 2018. *Synchronous Speed*. [Online] Available at: https://circuitglobe.com/synchronous-speed.html [Geopend May 2020].

Danish Wind Industry Association, 2003. *Changing Generator Rotational Speed*. [Online]

Available at: http://xn--drmstrre-64ad.dk/wp-content/wind/miller/windpower%20web/en/tour/wtrb/genpoles.htm
[Geopend May 2020].

Dasguptaa, K., Mandalb, S. K. & Panc, S., 2012. Dynamic analysis of a low speed high torque hydrostatic drive using steady-state characteristics. *Mechanism and Machine Theory,* Volume 52, pp. 1-17.

Electropaedia, sd *Electrical Machines - Generators*. [Online]
Available at: https://www.mpoweruk.com/generators.htm
[Geopend March 2020].

Esterhuizen, R., 2019. *Comparative Study between Synchronous Generator and Doubly-Fed Induction Generator in Wind Energy Conversion Systems,* sl: sn

Gemiddelden, sd *Gemiddelde watertemperatuur Noordzee*. [Online]
Available at: https://gemiddelden.nl/weer/gemiddelde-watertemperatuur-noordzee/
[Geopend May 2020].

Guo, B., Song, S., Ghalambor, A. & Ran Lin, T., 2013. Introduction to Flexible Pipelines. In: *Offshore Pipelines : Design, Installation, and Maintenance*. sl:Elsevier Science & Technology, p. 128.

Hansen, L. H. et al., 2001. *Conceptual survey of Generators and Power Electronics for Wind Turbines,* sl: DTU.

Hydraulics & Pneumatics, 2014. *Fundamentals of Hydraulic Motors*. [Online]
Available at: https://www.hydraulicspneumatics.com/technologies/hydraulic-pumps-motors/article/21884401/fundamentals-of-hydraulic-motors
[Geopend May 2020].

Jain, S. V. & Patel, R. N., 2014. Investigations on pump running in turbine mode: A review of the state-of-the-art. *Renewable and Sustainable Energy Reviews,* Volume 30, pp. 841-868.

Laguna, A., Van Wingerder, J. & Diepeveen, N., 2014. Analysis of dynamics of fluid power drive-trains for variable speed wind turbines: parameter study. *IET Renewable Power Generation,* 8(4), pp. 398-410.

MathWorks, 2006. *Fixed-Displacement Motor*. [Online]
Available at:
https://nl.mathworks.com/help/physmod/hydro/ref/hydraulicfluid.html
[Geopend April 2020].

MathWorks, 2006. *Hydraulic Fluid*. [Online]
Available at:
https://nl.mathworks.com/help/physmod/hydro/ref/hydraulicfluid.html
[Geopend April 2020].

MathWorks, 2009. *Hydraulic Resistive Tube*. [Online]
Available at:

https://nl.mathworks.com/help/physmod/simscape/ref/hydraulicresistivetube.html [Geopend April 2020].

Michael, P. W. et al., 2012. Lubricant Chemistry and Rheology Effects on Hydraulic Motor Starting Efficiency. *Tribology Transactions,* 55(5), pp. 549-557.

Neutrium, 2012. *Absolute Roughness of Pipe Material.* [Online]
Available at: https://neutrium.net/fluid_flow/absolute-roughness/
[Geopend April 2020].

North Sea Wind Power Hub, 2019. *Modular Hub-And-Spoke Concept To Facilitate Large Scale Offshore Wind.* [Online]
Available at: https://northseawindpowerhub.eu/wp-content/uploads/2019/11/NSWPH-Drieluik-Herdruk_v01.pdf
[Geopend 12 March 2020].

Quaker Chemical Corporation, 2020. *Synthetic Water Free Fluids (HFD-U).* [Online]
Available at: https://www.quintolubric.com/product-category/synthetic-water-free-fluids-hfd-u/
[Geopend May 2020].

Ra, R., Agoramb, C. A., Adithya, P. & Vanitha, V., 2015. Design and Analysis of Brushless Doubly Fed Induction Generator. *Elsevier Ltd.* .

Rotary Power, 2018. *How does a radial piston motor work?.* [Online]
Available at: https://rotarypower.com/how-does-a-radial-piston-motor-work/
[Geopend April 2020].

Sargent, R. G., 2013. Verification and validation of simulation models. *Journal of Sim,* 7(1), pp. 12-14.

Schachner, J., 2004. *Power Connections For Offshore Wind,* Delft: TU Delft.

Shahzad, U., 2012. The Need For Renewable Energy Sources. *International Journal of Information Technology and Electrical Engineering*.

Thirumalai, S. & Chenniappan, S., 2017. Performance Analysis of Wind Driven Generators. *Journal of Computational and Theoretical Nanoscience,* Volume 14, pp. 1-6.

van Kessel, T., 2020. *Simulation of the energy flow of an offshore,* Groningen: sn

van Rooij, M., 2020. [Illustraties] (Ocean Grazer).

Zhang, Z. et al., 2013. High-power generators for offshore wind turbines. *Energy Procedia ,* Volume 35, pp. 52-61.

19. Appendices

19.1. Appendix A: Alternating current vs Direct Current connection to the grid

To send the generated electricity to the mainland, alternating current (AC) or direct current (DC) can be utilized. For different applications, different types of currents can be used. Studies have demonstrated that offshore wind energy parks both use AC and DC to transmit the generated electricity to the mainland. The most important criterion for the selection of either AC or DC is the distance that must be covered by the cables. It is demonstrated that for a distance larger than 100 km, DC is best used. Whereas for shorter distances, AC is preferable. Therefore, depending on the location of the OG 3.0 design, it can be decided whether AC or DC is must be generated (Schachner, 2004).

19.2. Appendix B: power loss in the hydraulic tube

```
% plot power loss hydraulic tube
t =
time(out.simlogenergyloss.Fixed_Displacement_Motor1.mechanical_power.series
);
p = values(out.simlogenergyloss.Hydraulic_Resistive_Tube1.p.series);
q = values(out.simlogenergyloss.Hydraulic_Resistive_Tube1.q.series);
plot(t,p.*q)
```

19.3. Appendix C: power loss hydraulic motor

```
%difference hydraulic power input motor and mechanical power output
t =
time(out.simlogenergyloss.Fixed_Displacement_Motor1.mechanical_power.series
);
MechPower =
values(out.simlogenergyloss.Fixed_Displacement_Motor1.mechanical_power.seri
es);
HydPower =
values(out.simlogenergyloss.Fixed_Displacement_Motor1.hydraulic_power.serie
s);
plot(t,HydPower-MechPower)
```

19.4. Appendix D: Efficiency calculation hydraulic motor

```
%Plot hydraulic motor efficiency
t =
time(out.simlogenergyloss.Fixed_Displacement_Motor1.mechanical_power.series
);
MechPower =
values(out.simlogenergyloss.Fixed_Displacement_Motor1.mechanical_power.seri
es);
HydPower =
values(out.simlogenergyloss.Fixed_Displacement_Motor1.hydraulic_power.serie
s);
```

```
plot(t,MechPower./HydPower);
```

19.5. Appendix E: power loss Simscape model

```
%plot the power loss in the Simscape model
t =
time(out.simlogenergyloss.Fixed_Displacement_Motor1.mechanical_power.series
);
p = values(out.simlogenergyloss.Hydraulic_Resistive_Tube1.p.series);
q = values(out.simlogenergyloss.Hydraulic_Resistive_Tube1.q.series);
MechPower =
values(out.simlogenergyloss.Fixed_Displacement_Motor1.mechanical_power.seri
es);
HydPower =
values(out.simlogenergyloss.Fixed_Displacement_Motor1.hydraulic_power.serie
s);
plot(t,(p.*q)/1000+(HydPower-MechPower))
```

19.6. Appendix F: Efficiency calculation hydraulic tube and hydraulic motor

```
%Plot efficiency of the simscape model
t =
time(out.simlogenergyloss.Fixed_Displacement_Motor1.mechanical_power.series
);
MechPower =
1000*values(out.simlogenergyloss.Fixed_Displacement_Motor1.mechanical_power
.series);
flowrate = values(out.simlogenergyloss.Hydraulic_Resistive_Tube1.q.series);
Pressinput =
values(out.simlogenergyloss.Hydraulic_Pressure_Source.p.series);
plot(t,MechPower./(Pressinput.*flowrate));
```

19.7. Appendix G: manual analytical calculations of hydraulic tube pressure loss

$$v = \frac{4q}{\pi D_H^2} = \frac{4*60.0e^{-3}}{\pi*0.35^2} = 0.62 \text{ m/s}$$

$$Re = \frac{vD_H}{\nu} = \frac{0.62*0.35}{51.2014e^{-6}} = 4.2e^3$$

Therefore, the flow is turbulent.

$$f = \left(-1.8log_{10}\left(\frac{6.9}{Re} + \left(\frac{\frac{r}{D_H}}{3.7}\right)^{1.11}\right)\right)^{-2}$$

$$f = \left(-1.8log_{10}\left(\frac{6.9}{4.2e^3} + \left(\frac{\frac{6.0e^{-6}}{0.35}}{3.7}\right)^{1.11}\right)\right)^{-2} = 0.040$$

$\Delta p = \frac{fL\rho v^2}{2D_H} = \frac{0.040*70*842.96*0.62^2}{2*035}$=1296 Pa

19.8. Appendix H: manual analytical calculations of hydraulic motor leakage and friction

$T_{friction} = (T_0 + K_{TP}|\Delta p_m|) = 36000 + 0.00044 * 33.3e^6 = 5.1e^4$Nm

$T_{ideal} = D\Delta p_m = 0.138686 * 33.3e^6$=$4.62e^6$Nm/rev

$K_{HP} = \frac{\nu_{nom}\rho_{nom}\omega_{nom}D}{\rho\nu\Delta p_{nom}}\left(\frac{1}{\eta_v} - 1\right) = \frac{51.2014e^{-6}*842.96*26*0.138686}{51.2014e^{-6}*842.96*33e^6*60}\left(\frac{1}{0.996} - 1\right)$ =$8.0e^{-12}$

$q_{leak} = K_{HP}\Delta p_m$=$8.0e^{-12} * 33.3e^6 = 2.67 * e^{-4}$ m³/s

$q_{ideal} = D\omega_{ideal} = \frac{0.138686*26}{60} = 0.060$ m³/s

$q = q_{ideal} + q_{leak} = 0.060 + 2.67 * e^{-4} = 0.060$ m³/s

19.9. Appendix I: Component overview Simscape model